Available online at www.sciencedirect.com
SCIENCE DIRECT®
Physica D 191 (2004) 49–80
PHYSICA D
www.elsevier.com/locate/physd

Variational principles, Lie point symmetries, and similarity solutions of the vector Maxwell equations in non-linear optics

Garry Webb [a], Mads Peter Sørensen [b,*], Moysey Brio [b], Aramis R. Zakharian [b], Jerome V. Moloney [b]

[a] *Institute of Geophysics and Planetary Physics, University of California Riverside, Riverside, CA 92521, USA*
[b] *Department of Mathematics, Arizona Center for Mathematical Sciences, University of Arizona, Tucson, AZ 85721, USA*

Received 25 October 2001; received in revised form 10 June 2003; accepted 29 October 2003
Communicated by C.K.R.T. Jones

Abstract

The vector Maxwell equations of non-linear optics coupled to a single Lorentz oscillator and with instantaneous Kerr non-linearity are investigated by using Lie symmetry group methods. Lagrangian and Hamiltonian formulations of the equations are obtained. The aim of the analysis is to explore the properties of Maxwell's equations in non-linear optics, without resorting to the commonly used non-linear Schrödinger (NLS) equation approximation in which a high frequency carrier wave is modulated on long length and time scales due to non-linear sideband wave interactions. This is important in femto-second pulse propagation in which the NLS approximation is expected to break down. The canonical Hamiltonian description of the equations involves the solution of a polynomial equation for the electric field E, in terms of the canonical variables, with possible multiple real roots for E. In order to circumvent this problem, non-canonical Poisson bracket formulations of the equations are obtained in which the electric field is one of the non-canonical variables. Noether's theorem, and the Lie point symmetries admitted by the equations are used to obtain four conservation laws, including the electromagnetic momentum and energy conservation laws, corresponding to the space and time translation invariance symmetries. The symmetries are used to obtain classical similarity solutions of the equations. The traveling wave similarity solutions for the case of a cubic Kerr non-linearity, are shown to reduce to a single ordinary differential equation for the variable $y = E^2$, where E is the electric field intensity. The differential equation has solutions $y = y(\xi)$, where $\xi = z - st$ is the traveling wave variable and s is the velocity of the wave. These solutions exhibit new phenomena not obtainable by the NLS approximation. The characteristics of the solutions depends on the values of the wave velocity s and the energy integration constant ϵ. Both smooth periodic traveling waves and non-smooth solutions in which the electric field gradient diverges (i.e. solutions in which $|E_\xi| \to \infty$ at specific values of E, but where $|E|$ is bounded) are obtained. The traveling wave solutions also include a kink-type solution, with possible important applications in femto-second technology.

PACS: 02.20.Sv; 42.65.−k; 42.65.Re; 42.70.Mp

Keywords: Non-linear optics; Vector Maxwell's equations; Similarity solutions; Traveling waves

* Corresponding author. Present address: Department of Informatics and Mathematical Modelling, Technical University of Denmark, Richard Petersens Plads, DK-2800 Kgs. Lyngby, Denmark. Tel.: +45-4525-3094; fax: +45-4593-1235.
E-mail address: mps@imm.dtu.dk (M.P. Sørensen).
URL: http://www.imm.dtu.dk.

0167-2789/$ – see front matter © 2003 Elsevier B.V. All rights reserved.
doi:10.1016/j.physd.2003.10.014

1. Introduction

Most theoretical investigations of optical pulse propagation in fibers have been conducted by using the non-linear Schrödinger (NLS) equation or extended versions of the NLS equation. This approximation is very accurate for cases with a slowly varying envelope, shaping the carrier wave pulse [1,2]. However, for very short femto-second optical pulses a first principles approach in which the basic vector Maxwell equations are solved, coupled with a variety of resonant Lorentz oscillator models for the dielectric medium has been suggested [3]. In this approach, Maxwell's equations are solved without invoking weakly non-linear asymptotics used in the NLS approach, in which the high frequency carrier wave is modulated by a slowly varying envelope. The Lorentz models can involve one or more linear or non-linear oscillators describing the polarization electric field **P**. By solving Maxwell's equations coupled to the Lorentz oscillator equations directly, the slowly varying envelope assumption of the NLS approach need not be utilized. However, Hile [1] has shown, that even for cases where the NLS approximation should fail from a strictly mathematical point of view (i.e., when the frequencies of the carrier wave and the envelope are comparable), it nevertheless works surprisingly well, at least in the nano-second regime.

We focus on the properties of the Maxwell–Lorentz system, which are fundamentally and qualitatively different from that obtained using the NLS equation approach. We consider the simplest case of Maxwell's equations in one Cartesian space dimension coupled to a single resonant oscillator describing the coupling of the polarization electric field **P** to the electric field **E**. The model assumes that the displacement current D is related to the electric field strength E and polarization P by a constitutive relation of the form $D = E + P + aE^{2\sigma+1}$ (a and σ are the positive constants).

The model equations are expressed in terms of both Lagrangian and Hamiltonian variational principles. The Hamiltonian formulation of the equations involves the solution of a polynomial equation for the electric field E in terms of the canonical variables. In order to circumvent this problem non-canonical Poisson bracket formulations of the equations are investigated in which E is one of the non-canonical variables (Section 2).

The Lie point symmetries admitted by the equations are obtained in Section 3 (the equations are also shown to possess discrete, non-Lie symmetries). The Lie symmetries are used in conjunction with Noether's theorem (e.g. [7,8]) to determine four conservation laws for the system, including the electromagnetic momentum and energy conservation laws associated with the space and time translation symmetries admitted by the equations. The interesting question of whether the equations admit generalized Lie symmetries is left as an open question. Our analysis also does not address the important question of whether the equations are integrable, or admit a bi-Hamiltonian or multi-Hamiltonian structure which is a hallmark of completely integrable systems (e.g. [8,18]).

The Lie point symmetries are used to derive classical similarity solutions of the equations (Section 4), using the standard method described by Ovsjannikov [9], Ibragimov [10], Bluman and Kumei [7] and Olver [8].

The traveling wave similarity solutions are investigated in Section 5. For this class of solutions, the equations can be reduced to a single first order ordinary differential equation (ODE) for the electric field E as a function of the traveling wave variable $\xi = z - st$, where s is the velocity of the wave. If the integration constant, c_1, involved in integrating Ampere's equation is set equal to zero, the differential equation is more naturally expressed in terms of $y = E^2$. Both canonical and non-canonical Poisson bracket descriptions of the traveling waves are obtained. The differential equation for $y = y(\xi)$ is investigated in detail for the case of a cubic, Kerr non-linearity ($\sigma = 1$). The first order ODE for $y = y(\xi)$, is shown to develop shocks in the electric field ($|E_\xi| \to \infty$ as $y \to y_c = (1 - s^2)/s^2$ and $E \to E_c = y_c^{1/2}$). For a special choice of the energy integration constant ϵ, the singularity at $y = y_c$ in the denominator of the ODE is cancelled by a similar factor in the numerator, and leads to a special critical solution that passes smoothly through the critical point. A further, exact kink-type, implicit solution is also obtained. The kink solution corresponds to a heteroclinic orbit connecting two saddles in the (E, p)-phase plane, where $p = P_\xi$ is the canonical momentum. Numerical simulations are carried out to test the stability of the solutions.

Section 6 concludes with a summary and discussion.

2. Variational formulations

In this section we first discuss the model equations and the underlying physical assumptions (Section 2.1) and show that the system can be reduced to a single non-linear wave equation for the magnetic potential $\mathcal{A}$, in which the non-linear term is due to the Kerr non-linearity, and the wave dispersion is due to the effects of the Lorentz oscillator. In Section 2.2, the model equations are expressed in terms of Lagrangian and Hamiltonian variational principles. Both canonical and non-canonical Poisson bracket formulations of the equations are obtained.

2.1. Magnetic potential formulation

The equations of the model consist of Maxwell's equations coupled to a single Lorentz oscillator governing the polarization field **P**, in which the oscillator is driven by the electric field **E**. The equations of the model in dimensionless physical variables have the form[4]:

$$B_t + E_z = 0, \tag{2.1}$$

$$D_t + B_z = 0, \tag{2.2}$$

$$D = E + \frac{E^{2\sigma+1}}{2\sigma+1} + P, \tag{2.3}$$

$$P_{tt} + P - \alpha E = 0. \tag{2.4}$$

Here the residual Raman molecular vibration has been neglected. We assume a transverse plane wave propagating along the z-axis in which the electric field $\mathbf{E} = (E(z,t),0,0)^{\mathrm{T}}$, displacement current $\mathbf{D} = (D(z,t),0,0)^{\mathrm{T}}$ and polarization $\mathbf{P} = (P(z,t),0,0)^{\mathrm{T}}$ all lie along the x-axis and the magnetic field induction $\mathbf{B} = (0, B(z,t),0)^{\mathrm{T}}$ lies along the y-axis. The displacement current D in (2.3) depends non-linearly on the electric field E, and linearly on the polarization P. The Lorentz oscillator equation (2.4) shows that the polarization oscillations are driven by the electric field E, where the coupling parameter $\alpha = (\varepsilon_s - \varepsilon_\infty)/\varepsilon_\infty$. Here ε_s and ε_∞ are the static permittivity and linear permittivity in the medium, respectively [4]. The non-linear term in Eq. (2.3), i.e. $E^{2\sigma+1}/(2\sigma+1)$, is the instantaneous Kerr non-linearity with σ being an integer. For cubic non-linearity $\sigma = 1$ and for quintic non-linearity $\sigma = 2$. Eqs. (2.1) and (2.2) are Faraday's law, and Ampere's equation, respectively.

Introducing potentials ϕ and $\mathcal{A}$ for the electric and magnetic fields E and B:

$$E = \phi_z, \qquad B = \mathcal{A}_z. \tag{2.5}$$

Faraday's law (2.1) can be written as $(E + \mathcal{A}_t)_z = 0$. Thus

$$B = \mathcal{A}_z, \qquad E = -\mathcal{A}_t, \tag{2.6}$$

are representations for B and E in terms of the magnetic potential $\mathcal{A}$. In this representation of the fields E and B, Faraday's law (2.1) is automatically satisfied, as a consequence of the integrability condition $\mathcal{A}_{zt} = \mathcal{A}_{tz}$. Thus, (2.1)–(2.4) reduce to the system:

$$\frac{\partial}{\partial t}\left(-\mathcal{A}_t - \frac{\mathcal{A}_t^{2\sigma+1}}{2\sigma+1} + P\right) + \mathcal{A}_{zz} = 0, \tag{2.7}$$

$$P_{tt} + P + \alpha \mathcal{A}_t = 0 \tag{2.8}$$

for $\mathcal{A}$ and P.

Assuming $P(z, 0) = P_t(z, 0) = 0$, (2.8) can be integrated to yield the solution for P as a convolution integral in the form:

$$P(z, t) = -\alpha \int_0^t \frac{\partial \mathcal{A}(z, t')}{\partial t'} \sin(t - t')\, \mathrm{d}t'. \tag{2.9}$$

Using (2.9) in (2.7) then yields the non-linear wave equation:

$$\mathcal{A}_{zz} - (1 + \mathcal{A}_t^{2\sigma})\mathcal{A}_{tt} - \alpha \int_0^t \frac{\partial \mathcal{A}(z, t')}{\partial t'} \cos(t - t')\, \mathrm{d}t' = 0 \tag{2.10}$$

for $\mathcal{A}$. The non-linear term $\mathcal{A}_t^{2\sigma}\mathcal{A}_{tt}$ in (2.10) is due to the Kerr non-linearity in the relation between D and E. The wave equation (2.10) is dispersive due to the convolution integral term which is due to the oscillatory coupling of the polarization field P to the electric field E in the Lorentz model. Thus, (2.10) suggests that the interplay between non-linear pulse steepening and dispersion will play an important role in the Maxwell system (2.1)–(2.4).

A more general version of a non-linear wave equation for $\mathcal{A}$ obtained by eliminating P from (2.7) and (2.8) is

$$\left(\frac{\partial^2}{\partial t^2} + 1\right)[\mathcal{A}_{zz} - (1 + \mathcal{A}_t^{2\sigma})\mathcal{A}_{tt}] - \alpha \mathcal{A}_{tt} = 0. \tag{2.11}$$

Unlike (2.10), Eq. (2.11) does not assume special initial data for P and P_t.

2.2. Variational principles

The system of Eqs. (2.7) and (2.8) can be obtained by requiring that the action:

$$\mathcal{L} = \int_{-\infty}^{\infty} \mathrm{d}z \int_{-\infty}^{\infty} \mathrm{d}t\, L, \tag{2.12}$$

be stationary, where

$$L = \frac{1}{2}\mathcal{A}_t^2 + \frac{\mathcal{A}_t^{2\sigma+2}}{(2\sigma + 1)(2\sigma + 2)} - \frac{1}{2}\mathcal{A}_z^2 + \frac{P_t^2 - P^2}{2\alpha} - \mathcal{A}_t P, \tag{2.13}$$

is the Lagrangian density.

The Maxwell system (2.7) and (2.8) can be written in Hamiltonian form by using the canonical coordinates:

$$q_1 = \mathcal{A}, \qquad q_2 = P, \tag{2.14}$$

and the canonical momenta

$$p_1 = \frac{\partial L}{\partial \mathcal{A}_t} = \mathcal{A}_t + \frac{\mathcal{A}_t^{2\sigma+1}}{2\sigma + 1} - q_2, \tag{2.15}$$

$$p_2 = \frac{\partial L}{\partial P_t} = \frac{P_t}{\alpha}. \tag{2.16}$$

The Hamiltonian density H is given by the standard Legendre transformation:

$$H = \sum_{k=1}^{2} p_k q_{k,t} - L = \frac{1}{2}\mathcal{A}_t^2 + \frac{\mathcal{A}_t^{2\sigma+2}}{2\sigma + 2} + \frac{1}{2}\mathcal{A}_z^2 + \frac{P_t^2}{2\alpha} + \frac{P^2}{2\alpha}, \tag{2.17}$$

and the Hamiltonian functional $\mathcal{H} = \int_{-\infty}^{\infty} H \, dz$. Note that H can be written in terms of the canonical coordinates by solving (2.15) for $\mathcal{A}_t$, i.e., $\mathcal{A}_t = f(p_1 + q_2)$, where the function f satisfies the polynomial equation:

$$Y(f) = \frac{f^{2\sigma+1}}{2\sigma+1} + f = p_1 + q_2. \tag{2.18}$$

Hence

$$H = \frac{1}{2}f^2 + \frac{f^{2\sigma+2}}{2\sigma+2} + \frac{1}{2}\left(\frac{\partial q_1}{\partial z}\right)^2 + \frac{\alpha p_2^2}{2} + \frac{q_2^2}{2\alpha}, \tag{2.19}$$

is the form of H in terms of the canonical variables. Hamilton's equations

$$\frac{\partial q_j}{\partial t} = \frac{\delta \mathcal{H}}{\delta p_j}, \qquad \frac{\partial p_j}{\partial t} = -\frac{\delta \mathcal{H}}{\delta q_j} \quad (j = 1, 2), \tag{2.20}$$

are equivalent to the Maxwell system (2.7) and (2.8), when due account is taken of the implicit equation (2.18) for f.

In (2.18) $Y'(f) = f^{2\sigma} + 1 > 0$ (we assume f is real), and hence $Y(f)$ is a monotonic increasing function of f if σ is a positive integer. This means that there is a one–one relation between $Y(f) \equiv p_1 + q_2$ and $f = -E$. In other words, there is only one real root of Eq. (2.18) for f for real $p_1 + q_2$. However, in more complicated constitutive relations between the electric displacement D and E in (2.4), $Y(f)$ might not be a monotone function of f. Only real roots of (2.18) for $f \equiv -E$ are physically relevant. For example, for $\sigma = 1$, (2.18) is a cubic equation, whereas for $\sigma = 2$ the equation is a quintic equation for f. For the case $\sigma = 1$, the cubic (2.18) has one real root f_1 and two complex conjugate roots f_2 and f_3. The relevant real root f_1, can be written in the form:

$$f = f_1 = [C + (C^2 + 1)^{1/2}]^{1/3} - [C + (C^2 + 1)^{1/2}]^{-1/3}, \tag{2.21}$$

where

$$C = \tfrac{3}{2}(p_1 + q_2) \tag{2.22}$$

[11, p. 17, Formula 3.8.2; 16, p. 90]. Thus, for $\sigma = 1$ (cubic Kerr non-linearity), there is only one real solution for f, and only one real Hamiltonian in (2.19).

The relation (2.18) indicates that in general E will be a multi-valued function of $p_1 + q_2$, but we require E to be a single valued function of z, at a fixed time t for a physically valid solution. This same problem also arises in the canonical Hamiltonian description of the traveling wave solutions of the Maxwell–Lorentz system (2.1)–(2.4) discussed in Section 5. For these solutions, all physical variables only depend on the traveling wave variable $\xi = z - st$. The equations can be represented as a two-dimensional Hamiltonian system, with Hamiltonian $H_0(q, p)$, where $q = P$ and $p = P_\xi$. The canonical coordinate q in the model is a polynomial in the electric field E. To write the equations in terms of canonical coordinates, it is necessary to solve the polynomial equation to determine the electric field in terms of q. In the case of a Kerr cubic non-linearity, there are up to three real solutions for the electric field $E = E(q)$. In order to circumvent these problems of multi-valued solutions for $E = E(q)$, it is simpler to change from a canonical Poisson bracket description, to a non-canonical Poisson bracket description in which E is one of the non-canonical variables.

The occurrence of multiple valued functions in the Hamiltonian equations (2.18)–(2.22) is reminiscent of multi-valued Clebsch variables that can arise in canonical formulations of the equations of ideal fluid mechanics. For example, Zakharov and Kuznetsov [20], in discussing knotted flows in ideal, incompressible fluid mechanics use the Clebsch representation $\mathbf{v} = \nabla\phi + \lambda\nabla\mu$ for the fluid velocity $\mathbf{v}$, and $\boldsymbol{\omega} = \nabla \times \mathbf{v} = \nabla\lambda \times \nabla\mu$ is the fluid vorticity. The Clebsch potential ϕ is associated with potential flow and the Clebsch potential μ is identified with the

conserved fluid velocity circulation moving with a fluid element in Kelvin's theorem. Zakharov and Kuznetsov note that the Clebsch potentials λ and μ in general are multiple valued functions, and hence it is appropriate to introduce alternative formulations and variables in which the flow field and vorticity are uniquely defined.

In order to construct a non-canonical Poisson bracket formulation of the equations, we first note that Hamilton's equation (2.20) can be written in the canonical Poisson bracket form:

$$\frac{\partial \boldsymbol{\eta}}{\partial t} = \{\boldsymbol{\eta}, \mathcal{H}\}_c, \tag{2.23}$$

where $\boldsymbol{\eta} = (q_1, q_2, p_1, p_2)^{\mathrm{T}}$ and

$$\{\mathcal{F}, \mathcal{G}\}_c = \int_{-\infty}^{\infty} \mathrm{d}z \sum_{j=1}^{2} \left(\frac{\delta \mathcal{F}}{\delta q_j} \frac{\delta \mathcal{G}}{\delta p_j} - \frac{\delta \mathcal{F}}{\delta p_j} \frac{\delta \mathcal{G}}{\delta q_j} \right). \tag{2.24}$$

The Poisson bracket (2.24) can also be written in the form:

$$\{\mathcal{F}, \mathcal{G}\}_c = \int_{-\infty}^{\infty} \mathrm{d}z \, \frac{\delta \mathcal{F}}{\delta \eta^{\alpha}} J_c^{\alpha\beta} \frac{\delta \mathcal{G}}{\delta \eta^{\beta}}, \tag{2.25}$$

where

$$\mathbf{J}_c = \begin{pmatrix} \mathbf{O}_2 & \mathbf{I}_2 \\ -\mathbf{I}_2 & \mathbf{O}_2 \end{pmatrix}. \tag{2.26}$$

Here, $\mathbf{O}_2$ and $\mathbf{I}_2$ denote the zero 2×2 matrix and the unit 2×2 matrix, respectively. $\mathbf{J}_c$ is known as the canonical symplectic operator or matrix. One can also think of $\mathbf{J}_c$ as defining the symplectic metric (e.g. [17]). Note that $\mathbf{J}_c$ is a skew-symmetric matrix with $\mathbf{J}^{\mathrm{T}} = -\mathbf{J}$, and the Poisson bracket (2.25) satisfies the Jacobi identity [17,19,20].

One can construct a non-canonical Poisson bracket by transforming the canonical Poisson bracket to the new non-canonical coordinates (e.g. [19–23]). However, one may still be confronted with situations in which the solutions of the equations evolve to produce shocks (e.g. in compressible gas dynamics, or in the inviscid Burgers equation, the solutions can become multiple valued, unless one inserts a shock to restore the uniqueness of the weak solution). Using the non-canonical physical variables

$$\tilde{\boldsymbol{\eta}} = (E, B, P, p_2) \quad \text{where} \quad p_2 = \frac{P_t}{\alpha}, \tag{2.27}$$

the Maxwell system (2.1)–(2.4) can be written in the Poisson bracket form:

$$\frac{\partial \tilde{\boldsymbol{\eta}}}{\partial t} = \{\tilde{\boldsymbol{\eta}}, \mathcal{H}\}, \tag{2.28}$$

where $\mathcal{H}$ is the Hamiltonian functional. The non-canonical Poisson bracket in (2.28) is defined by the equation $\{\tilde{\mathcal{F}}, \tilde{\mathcal{G}}\} := \{\mathcal{F}, \mathcal{G}\}_c$, where $\tilde{\mathcal{F}}[\tilde{\boldsymbol{\eta}}] = \mathcal{F}[\boldsymbol{\eta}]$ is the functional obtained by writing the functional $\mathcal{F}$ in terms of the new variables $\tilde{\boldsymbol{\eta}}$ and similarly, for $\tilde{\mathcal{G}}$. Thus, to obtain the explicit form of the non-canonical Poisson bracket it is necessary to determine the transformation of variational derivatives between the new and the old variables. These transformations are

$$\frac{\delta \mathcal{F}}{\delta q_1} = -D_z \left(\frac{\delta \tilde{\mathcal{F}}}{\delta B} \right), \qquad \frac{\delta \mathcal{F}}{\delta q_2} = \frac{\delta \tilde{\mathcal{F}}}{\delta P} + \frac{\delta \tilde{\mathcal{F}}}{\delta E} \frac{\partial E}{\partial q_2}, \qquad \frac{\delta \mathcal{F}}{\delta p_1} = \frac{\delta \tilde{\mathcal{F}}}{\delta E} \frac{\partial E}{\partial p_1}, \qquad \frac{\delta \mathcal{F}}{\delta p_2} = \frac{\delta \tilde{\mathcal{F}}}{\delta p_2}, \tag{2.29}$$

where D_z is the total derivative operator with respect to z. Using (2.29) to replace the functional derivatives $\delta \mathcal{F}/\delta \eta$ in (2.25) we obtain:

$$\{\tilde{\mathcal{F}}, \tilde{\mathcal{G}}\} = \int_{-\infty}^{\infty} \mathrm{d}z \, \frac{\delta \tilde{\mathcal{F}}}{\delta \tilde{\eta}^{\alpha}} \tilde{J}^{\alpha\beta} \frac{\delta \tilde{\mathcal{G}}}{\delta \tilde{\eta}^{\beta}} \tag{2.30}$$

for the non-canonical Poisson bracket $\{\tilde{\mathcal{F}}, \tilde{\mathcal{G}}\}$, where

$$\tilde{\mathbf{J}} = \begin{pmatrix} 0 & -\zeta D_z & 0 & -\zeta \\ -D_z(\zeta \cdot) & 0 & 0 & 0 \\ 0 & 0 & 0 & 1 \\ \zeta & 0 & -1 & 0 \end{pmatrix}, \tag{2.31}$$

$$\zeta = \frac{\partial f}{\partial p_1} = \frac{\partial f}{\partial q_2} = (1 + E^{2\sigma})^{-1}. \tag{2.32}$$

The matrix operator $\tilde{\mathbf{J}}$ in (2.31) is a skew adjoint operator with respect to the symplectic inner product

$$\langle \mathbf{u}, \mathbf{v} \rangle = \int_{-\infty}^{\infty} u_{\alpha} v^{\alpha} \, \mathrm{d}z = \int_{-\infty}^{\infty} u_{\alpha} \tilde{J}^{\alpha\beta} v_{\beta} \, \mathrm{d}z. \tag{2.33}$$

In Appendix A, we show directly that the bracket (2.30) is skew-symmetric and that the Jacobi identity is satisfied, by using the results of Olver [8]. The Hamiltonian operator $\tilde{\mathbf{J}}$ in (2.31) is singular when $D_z\zeta \to \infty$. This occurs at points where the electric field gradient $D_z E \to \infty$, and it is then necessary to consider how to treat shocks in the electric field.

The set of non-canonical variables (2.27) is not unique. For example, one could also use the non-canonical variables $\hat{\boldsymbol{\eta}} = (q_1, q_2, E, p_2)^{\mathrm{T}} \equiv (\mathcal{A}, P, E, P_t/\alpha)^{\mathrm{T}}$. The non-canonical Poisson bracket in this case satisfies the conditions of skew-symmetry and the Jacobi identity, and the symplectic matrix operator $\hat{\mathbf{J}}$, depends on ζ, but not on the total z-derivative operator D_z.

3. Lie symmetries and conservation laws

In this section we obtain the Lie point symmetries of the Maxwell–Lorentz oscillator equations (2.1)–(2.4) or the equivalent system (2.7) and (2.8), and use the symmetries to obtain conservation laws for the equations by using Noether's theorem. We first present a short overview of the use of Lie symmetries in obtaining solutions of differential equations in Section 3.1. This also includes a discussion of Noether's first theorem in obtaining conservation laws for a system of differential equations that arise as a critical point of a Lagrangian variational principle (see e.g. [8, Chapter 5] for the Noether's first and second theorems on variational symmetries). The Lie point symmetries admitted by the Maxwell–Lorentz oscillator system (2.1)–(2.4) and its Lie algebra are obtained in Section 3.2. The symmetries are then used in conjunction with Noether's theorem to obtain conservation laws for the system. We identify the stress-energy tensor for the system associated with the momentum and energy conservation laws.

3.1. Basic results on Lie symmetries and differential equations

The general procedure to obtain Lie symmetries of differential equations, and their application to find conservation laws and analytic solutions of the equations are described in detail in several monographs on the subject (e.g. [7–10,12]) and in numerous papers in the literature (e.g. [15,24,25]).

Consider a system of differential equations in the dependent variables u^α $(1 \le \alpha \le m)$ and independent variables x^i $(1 \le i \le n)$ of the form:

$$\Omega^s(x^i, u^\alpha, u^\alpha_i, u^\alpha_{ij}, \dots) = 0, \quad 1 \le s \le k, \tag{3.1}$$

where the subscripts denote partial derivatives (e.g. $u^\alpha_i = \partial u^\alpha / \partial x_i$). To determine continuous symmetries of (3.1), it is useful to consider infinitesimal Lie transformations of the form:

$$x'^i = x^i + \epsilon\xi^i + \mathrm{O}(\epsilon^2), \qquad u'^\alpha = u^\alpha + \epsilon\phi^\alpha + \mathrm{O}(\epsilon^2), \tag{3.2}$$

that leave the equation system invariant to $\mathrm{O}(\epsilon)$. Lie point symmetries correspond to the case where the infinitesimal generators $\xi^i = \xi^i(x^i, u^\alpha)$ and $\phi^\alpha = \phi^\alpha(x^i, u^\alpha)$ depend only on the x^i and the u^α and not on the derivatives or integrals of the u^α. Generalized Lie symmetries are obtained in the case when the transformations (3.2) also depend on the derivatives or integrals of the u^α.

The infinitesimal transformations for the first and second derivatives to $\mathrm{O}(\epsilon)$ are given by the prolongation formulae:

$$u'^\alpha_i = u^\alpha_i + \epsilon\zeta^\alpha_i, \qquad u'^\alpha_{ij} = u^\alpha_{ij} + \epsilon\zeta^\alpha_{ij}, \tag{3.3}$$

where

$$\zeta^\alpha_i = D_i\hat{\phi}^\alpha + \xi^s u^\alpha_{si}, \qquad \zeta^\alpha_{ij} = D_i D_j\hat{\phi}^\alpha + \xi^s u^\alpha_{sij}. \tag{3.4}$$

Here

$$\hat{\phi}^\alpha = \phi^\alpha - \xi^s u^\alpha_s, \tag{3.5}$$

corresponds to the canonical Lie transformation for which $x'^i = x^i$ and $u'^\alpha = u^\alpha + \epsilon\hat{\phi}^\alpha$. The symbol D_i in (3.4) denotes the total derivative operator with respect to x^i. Similar formulae to (3.4) apply for the transformation of higher order derivatives.

The condition for invariance of the differential equation system (3.1) to $\mathrm{O}(\epsilon)$ under the Lie transformation (3.2) can be expressed in the form:

$$\mathcal{L}_X\Omega^s \equiv \tilde{X}\Omega^s = 0 \quad \text{whenever} \quad \Omega^s = 0, \quad 1 \le s \le k, \tag{3.6}$$

where

$$\tilde{X} = X + \zeta^\alpha_i \frac{\partial}{\partial u^\alpha_i} + \zeta^\alpha_{ij} \frac{\partial}{\partial u^\alpha_{ij}} + \cdots, \tag{3.7}$$

is the prolongation of the vector field

$$X = \xi^i \frac{\partial}{\partial x^i} + \phi^\alpha \frac{\partial}{\partial u^\alpha}, \tag{3.8}$$

associated with the infinitesimal transformation (3.2). The symbol $\mathcal{L}_X\Omega^s$ in (3.6) denotes the Lie derivative of Ω^s with respect to the vector field X (i.e. $\mathcal{L}_X\Omega^s = (\mathrm{d}\Omega^s/\mathrm{d}\epsilon)_{\epsilon=0}$).

The prolonged symmetry operator $\tilde{X}$ is related to the prolonged, canonical symmetry operator $\hat{X}$ by the equation

$$\tilde{X} = \hat{X} + \xi^i D_i. \tag{3.9}$$

The canonical symmetry operator (or the evolutionary symmetry with characteristic $\hat{\phi}$) corresponds to the symmetry transformation for which $x'^i = x^i$ and $u'^\alpha = u^\alpha + \epsilon\hat{\phi}^\alpha$. The prolonged symmetry operator $\hat{X}[\hat{\phi}]$ is given by

$$\hat{X}[\hat{\phi}] = \hat{\phi}^\alpha \frac{\partial}{\partial u^\alpha} + D_i\hat{\phi}^\alpha \frac{\partial}{\partial u^\alpha_i} + D_i D_j\hat{\phi}^\alpha \frac{\partial}{\partial u^\alpha_{ij}} + \cdots + D_{i_1} D_{i_2} \dots D_{i_s}\hat{\phi}^\alpha \frac{\partial}{\partial u^\alpha_{i_1 i_2 \dots i_s}} + \cdots. \tag{3.10}$$

The Lie bracket of two canonical symmetry operators with characteristics $\hat{\phi}_1$ and $\hat{\phi}_2$ is given by

$$[\hat{X}[\hat{\phi}_1], \hat{X}[\hat{\phi}_2]] = \hat{X}[\hat{\phi}_3] \quad \text{where } \hat{\phi}_3 = \hat{X}[\hat{\phi}_1]\hat{\phi}_2 - \hat{X}[\hat{\phi}_2]\hat{\phi}_1. \tag{3.11}$$

In addition, $[\hat{X}[\hat{\phi}], D_i] = 0$ and $[D_i, D_j] = 0$ [10]. Thus, the canonical symmetry operators form a Lie algebra, $\hat{L}$, which will be infinite dimensional if there is an infinite number of distinct $\hat{\phi}_j$. Ibragimov [10] shows that the algebra $\hat{L}$ is a subalgebra of $\tilde{L}$, the symmetry algebra of the prolonged vector fields $\tilde{X}$. In fact, $\hat{L}$ is isomorphic to the factor algebra $\tilde{L}/L_*$, where $L_* = \{X_* \in \tilde{L} : X_* = \xi^j_* D_j\}$ is a closed ideal in $\tilde{L}$ (i.e. $[\tilde{X}, X_*] \in L_*$ for all $X_* \in L_*$ and $\tilde{X} \in \tilde{L}$).

3.1.1. Classical similarity solutions

Lie point symmetries of the system (3.1) are determined by solving the overdetermined Lie determining equation (3.6) for the infinitesimal generators $\{\xi^i : 1 \le i \le n\}$ and the $\{\phi^\alpha : 1 \le \alpha \le m\}$. Classical similarity solutions of (3.1) are obtained by requiring the solution surfaces for the u^α are mapped onto the same set of surfaces, in the sense that $u'^\alpha(\mathbf{x}) = u^\alpha(\mathbf{x}')$. These conditions, to $O(\epsilon)$ yield the first order partial differential equations $\xi^i u^\alpha_i = \phi^\alpha$ (e.g. [15]), with characteristics being given by the group trajectories:

$$\frac{\mathrm{d}x^i}{\mathrm{d}\epsilon} = \xi^i \quad \text{and} \quad \frac{\mathrm{d}u^\alpha}{\mathrm{d}\epsilon} = \phi^\alpha, \quad 1 \le i \le n, \quad 1 \le \alpha \le m. \tag{3.12}$$

Integration of the group trajectories yield the invariants of the point Lie group admitted by the system, and these may be used to construct the classical similarity solutions of the system (3.1). Classical similarity solutions of the Maxwell–Lorentz system (2.1)–(2.4) are constructed by these methods in Section 4.

3.1.2. Noether's first theorem and the calculus of variations

In this subsection we consider differential equation systems that arise from critical point conditions for a Lagrangian action principle, in which the action is of the form:

$$J[u] = \int_R \mathrm{d}\mathbf{x}\, L(x^i, u^\alpha, u^\alpha_i, u^\alpha_{ij}, \dots). \tag{3.13}$$

At a critical point, the action is stationary, i.e.,

$$\delta J = J[u + \epsilon v] - J[u] = \int_R \mathrm{d}\mathbf{x}\, \delta L = 0, \tag{3.14}$$

where

$$\delta L \equiv L[u + \epsilon v] - L[u] = \epsilon(v^\gamma E_\gamma(L) + D_i W^i[u, v]) + O(\epsilon^2) \tag{3.15}$$

[7]. Thus, the critical point requirement $\delta J = 0$ is satisfied if the u^α satisfy the Euler–Lagrange equations:

$$E_\alpha[L] = \frac{\partial L}{\partial u^\alpha} - D_i\left(\frac{\partial L}{\partial u^\alpha_i}\right) + D_i D_j\left(\frac{\partial L}{\partial u^\alpha_{ij}}\right) - D_i D_j D_k\left(\frac{\partial L}{\partial u^\alpha_{ijk}}\right) + \cdots = 0, \tag{3.16}$$

provided that the surface term $\mathbf{W} \cdot \mathbf{n}$ that arises from integrating $D_i W^i$ by using Gauss's theorem vanishes on the boundary ∂R with outward unit normal $\mathbf{n}$ of the integration region R for $J[u]$. In (3.15) the boundary vector $W^i[u, v]$ is given by

$$\begin{aligned} W^i[\mathbf{u}, \mathbf{v}] = {} & v^\gamma\left[\frac{\partial L}{\partial u^\gamma_i} - D_j\left(\frac{\partial L}{\partial u^\gamma_{ij}}\right) + D_j D_k\left(\frac{\partial L}{\partial u^\gamma_{ijk}}\right) - \cdots\right] \\ & + v^\gamma_j\left[\frac{\partial L}{\partial u^\gamma_{ij}} - D_k\left(\frac{\partial L}{\partial u^\gamma_{ijk}}\right) + D_\ell D_k\left(\frac{\partial L}{\partial u^\gamma_{ijk\ell}}\right) - \cdots\right] + v^\gamma_{jk}\left[\frac{\partial L}{\partial u^\gamma_{ijk}} - D_s\left(\frac{\partial L}{\partial u^\gamma_{ijks}}\right) + \cdots\right] + \cdots. \end{aligned} \tag{3.17}$$

Thus, $W^i[u, v]$ will vanish on ∂R if $\delta u^\alpha = \epsilon v^\alpha$ and its normal derivatives all vanish on the boundary. In the above equations, $E_\alpha[L]$ defines the Euler operator E_α for the system. The Euler–Lagrange equations (3.16) constitute the differential equations $\Omega^s = 0$ $(1 \leq s \leq m)$ for the system in this case. The surface vector W^i plays a central role in Noether's theorem.

3.1.2.1. Noether's first theorem. One important idea in the proof of Noether's theorem is the result that two Lagrangian densities L_1 and L_2 that differ by a pure divergence have the same Euler–Lagrange equation (3.16). This property depends on the result that $E_\gamma[D_i F] = 0$ for any sufficiently smooth functional $F[u]$. Thus if $L_2 - L_1 = D_i A^i$, then $E_\alpha[L_1] = E_\alpha[L_2]$. This fact motivates the definition of a variational symmetry given below.

3.1.2.2. Definition. A canonical, generalized, Lie symmetry $x^* = x$, $u^{*\alpha} = u^\alpha + \epsilon\hat{\phi}^\alpha$ is called a *variational symmetry* of the action (3.13), if there exists a vector field **A** such that $\hat{X}L = D_i A^i$.

For a variational symmetry, we have to $O(\epsilon)$, that $L^* - L = \epsilon\hat{X}L = \epsilon D_i A^i$. Hence L^* and L differ by a pure divergence, which implies that to $O(\epsilon)$, L and L^* have the same Euler–Lagrange equations. This explains the origin of the definition of a variational symmetry.

Bluman and Kumei [7, Chapter 5] consider Boyer's version of Noether's theorem as well as the original version of the theorem given by Noether. These two versions of Noether's theorem are given below.

3.1.2.3. Boyer's version of Noether's theorem. Let $\hat{X}[\hat{\phi}]$ be the Lie symmetry operator corresponding to the generalized, canonical Lie transformation $x^{*i} = x^i$ and $u^{*\alpha} = u^\alpha + \epsilon\hat{\phi}^\alpha$. If $\hat{\phi}$ is a variational symmetry of the action (3.13) (i.e., if $\hat{X}[\hat{\phi}]L = D_i A^i$ for some vector field **A**), then for any solution u of the Euler–Lagrange equations $E_\gamma[L] = 0$, there is a corresponding conservation law:

$$D_i(W^i[u, \hat{\phi}] - A^i) = 0. \tag{3.18}$$

The proof of (3.18) depends on the result:

$$\hat{X}L = \hat{\phi}^\gamma E_\gamma[L] + D_i W^i[u, \hat{\phi}]. \tag{3.19}$$

The result (3.19) follows from (3.15) with $v^\gamma = \hat{\phi}^\gamma$ and the definition of $\hat{X}[\hat{\phi}]L$ as a Lie derivative. Using (3.19) in conjunction with the fact that $\hat{X}[\hat{\phi}]L = D_i A^i$ and noting $E_\gamma[L] = 0$ for u a solution of the Euler–Lagrange equation (3.16) establishes the theorem.

Note that the theorem in this form does not give a method to find variational symmetries. One can show that if $\hat{\phi}$ is a variational symmetry, then it is also a generalized symmetry of the Euler–Lagrange equation (3.16). However, not all symmetries of the Euler–Lagrange equations are necessarily variational symmetries.

Below is the original version of Noether's first theorem.

3.1.2.4. Noether's theorem. If the action (3.13) is invariant under a generalized Lie transformation (3.2) (i.e., $x' = x + \epsilon\xi^i$, $u'^\alpha = u^\alpha + \epsilon\phi^\alpha$), then for any solution u of the Euler–Lagrange equations $E_\gamma[L] = 0$, there is a corresponding conservation law:

$$D_i(W^i[u, \hat{\phi}] + \xi^i L) = 0 \tag{3.20}$$

(see e.g. [7, Chapter 5] for a proof). Thus, one can think of Noether's original version of the theorem as the special case of Boyer's version of the theorem when $A^i = -\xi^i L$.

3.2. Lie symmetries and conservation laws

The Lie symmetries of the Maxwell–Lorentz oscillator system (2.1)–(2.6) or the equivalent equation system (2.7) and (2.8) for $\mathcal{A}$ and P can be found by solving the Lie determining equation (3.6) for the infinitesimal generators of the Lie group. Below, we first write down the Lie determining equations for the system, and give the solutions of the determining equations that correspond to the point Lie group. The point Lie algebra of the system is briefly described, and the symmetries are then used to obtain conservation laws for the system by using Noether's theorem, as described in (3.13), etc.

3.2.1. Lie symmetries

The infinitesimal Lie transformations for the system (2.1)–(2.6) are of the form:

$$t' = t + \epsilon\xi^t, \quad z' = z + \epsilon\xi^z, \quad \mathcal{A}' = \mathcal{A} + \epsilon\phi^{\mathcal{A}}, \quad E' = E + \epsilon\phi^E, \quad B' = B + \epsilon\phi^B, \qquad P' = P + \epsilon\phi^P. \tag{3.21}$$

The corresponding canonical Lie symmetry generators $\hat{\phi}^E$, $\hat{\phi}^B$, $\hat{\phi}^P$ and $\hat{\phi}^{\mathcal{A}}$ are given by formulae analogous to (3.5). Thus

$$\hat{\phi}^w = \phi^w - \xi^t w_t - \xi^z w_z, \tag{3.22}$$

relates the canonical symmetry generator $\hat{\phi}^w$ to ϕ^w, where w can be any of the dependent variables E, B, P or $\mathcal{A}$.

The Lie determining equation (3.6) for the infinitesimal generators of the system (2.1)–(2.4) can be written in the form:

$$D_t\hat{\phi}^B + D_z\hat{\phi}^E = 0, \tag{3.23}$$

$$(1 + E^{2\sigma})D_t\hat{\phi}^E + 2\sigma E^{2\sigma-1}E_t\hat{\phi}^E + D_t\hat{\phi}^P + D_z\hat{\phi}^B = 0, \tag{3.24}$$

$$D_t^2\hat{\phi}^P + \hat{\phi}^P - \alpha\hat{\phi}^E = 0. \tag{3.25}$$

The auxiliary equation (2.6) giving B and E in terms of the magnetic potential $\mathcal{A}$ have Lie determining equations:

$$\hat{\phi}^B = D_z\hat{\phi}^{\mathcal{A}} \quad \text{and} \quad \hat{\phi}^E = -D_t\hat{\phi}^{\mathcal{A}}. \tag{3.26}$$

Note that these equations can also be written down in terms of the non-canonical symmetry generators ξ^t, ξ^z, ϕ^E, ϕ^B, ϕ^P and $\phi^{\mathcal{A}}$. It is straightforward to write down the Lie determining equations for the equivalent system of Eqs. (2.7) and (2.8) for $\mathcal{A}$ and P, but these equations are not necessary for the analysis.

For the case of Lie point symmetries, the non-canonical symmetry generators are assumed to depend only on (t, z, E, B, P) in (3.21)–(3.26). Using (3.22), this means that the canonical symmetry operators $\hat{\phi}^w$ ($w = E, B, P, \mathcal{A}$) can depend only on t, z and the first order space and time derivatives of E, B, P and $\mathcal{A}$. The determining equations (3.23)–(3.26) have solutions for the non-canonical symmetry generators of the form:

$$\xi^t = a_1, \quad \xi^z = a_2, \quad \phi^E = 0, \quad \phi^P = 0, \quad \phi^B = a_3, \quad \phi^{\mathcal{A}} = a_3 z + a_4, \tag{3.27}$$

where the $\{a_j : 1 \le j \le 4\}$ are constants. The corresponding canonical Lie symmetry generators are

$$\hat{\phi}^E = -a_1E_t - a_2E_z, \quad \hat{\phi}^P = -a_1P_t - a_2P_z, \quad \hat{\phi}^B = a_3 - a_1B_t - a_2B_z,$$
$$\hat{\phi}^{\mathcal{A}} = a_3 z + a_4 - a_1\mathcal{A}_t - a_2\mathcal{A}_z. \tag{3.28}$$

One can verify that the canonical symmetries (3.28) do in fact satisfy the Lie determining equations on the solution manifold of (2.1)–(2.6). For example,

$$D_t\hat{\phi}^B + D_z\hat{\phi}^E = -(a_1D_t + a_2D_z)(B_t + E_z). \tag{3.29}$$

Since $E_t + B_z = 0$ on the solution manifold, then the right handside of (3.29) is zero. Similarly, one can check that the solution (3.28) for the canonical Lie symmetries satisfies the other Lie determining equations (3.24)–(3.26) on the solution manifold.

The Lie point symmetry generators in (3.27) correspond to the time (a_1) and space (a_2) translation symmetries, the symmetry of invariance under translations in B (i.e. the transformation $B' = B + \epsilon a_3$) and the guage transformation symmetry for $\mathcal{A}$ (i.e. the symmetry for which $\mathcal{A}' = \mathcal{A} + \epsilon a_4$). In principle, Eqs. (3.23)–(3.26) could also admit generalized Lie symmetries that depend on the higher order derivatives of E, B and P. However, this possibility will not be investigated here.

The Eqs. (2.7) and (2.8) also admit the discrete, non-Lie symmetry transformation

$$t' = t, \qquad z' = z, \qquad \mathcal{A}' = -\mathcal{A}, \qquad P' = -P. \tag{3.30}$$

Another discrete symmetry is

$$t' = -t, \qquad z' = z, \qquad \mathcal{A}' = \mathcal{A}, \qquad P' = -P \tag{3.31}$$

(there may possibly be more discrete symmetries).

3.2.2. The point Lie algebra

The general vector field X in the point Lie algebra corresponding to the transformations (3.21) can be written in the form:

$$X = \sum_{i=1}^{4} a_i X_i, \tag{3.32}$$

where the basis vector fields $\{X_i : 1 \le i \le 4\}$ are

$$X_1 = \frac{\partial}{\partial t}, \qquad X_2 = \frac{\partial}{\partial z}, \qquad X_3 = z\frac{\partial}{\partial \mathcal{A}}, \qquad X_4 = \frac{\partial}{\partial \mathcal{A}}. \tag{3.33}$$

The only non-zero commutators $[X_i, X_j]$ of the point Lie algebra are

$$[X_2, X_3] = X_4 \quad \text{and} \quad [X_3, X_2] = -X_4. \tag{3.34}$$

Using (3.34), and noting $[X_4, X_4] = 0$, it follows that the Lie algebra is solvable.

3.2.3. Conservation laws

In this section both forms of Noether's first theorem as described in (3.13), etc. are used to obtain conservation laws for the system (2.7) and (2.8) of the form:

$$\frac{\partial W_j}{\partial t} + \frac{\partial F_j}{\partial z} = 0, \quad j = 1, 2, 3, 4. \tag{3.35}$$

Because the Lagrangian density L in (2.13) only involves first order derivatives of $\mathcal{A}$ and P, the surface flux functions $W^i[u, \hat{\phi}]$ ($i = 1, 2$) in (3.17) have the form:

$$W^1 = \hat{\phi}^{\mathcal{A}}\frac{\partial L}{\partial \mathcal{A}_t} + \hat{\phi}^{P}\frac{\partial L}{\partial P_t}, \qquad W^2 = \hat{\phi}^{\mathcal{A}}\frac{\partial L}{\partial \mathcal{A}_z} + \hat{\phi}^{P}\frac{\partial L}{\partial P_z}, \tag{3.36}$$

where $(x^1, x^2) = (t, z)$ are the independent variables. We derive the conservation laws associated with the four symmetry vector fields X_1, X_2, X_3 and X_4 below.

3.2.3.1. Time translation invariance (X_1). For this symmetry

$$\xi^t = 1, \qquad \xi^z = 0, \qquad \hat{\phi}^{\mathcal{A}} = -\mathcal{A}_t, \qquad \hat{\phi}^{P} = -P_t. \tag{3.37}$$

This symmetry leaves the action (2.12) invariant. Using (3.36) we obtain

$$W^1 = -\mathcal{A}_t\left(\mathcal{A}_t + \frac{\mathcal{A}_t^{2\sigma+1}}{2\sigma+1} - P\right) - \frac{P_t^2}{\alpha}, \qquad W^2 = \mathcal{A}_t\mathcal{A}_z. \tag{3.38}$$

Using Noether's theorem (3.20), the conserved density $W_1 = -(W^1 + L)$ and flux $F_1 = -W^2$ are given by

$$W_1 = \frac{1}{2}(E^2 + B^2) + \frac{E^{2\sigma+2}}{2\sigma+2} + \frac{1}{2\alpha}(P_t^2 + P^2), \tag{3.39}$$

$$F_1 = EB. \tag{3.40}$$

The conservation law (3.35) in this case is electromagnetic energy conservation law (Poynting's theorem) for a Kerr-medium.

3.2.3.2. Space translation invariance (X_2). In this case

$$\xi^t = 0, \qquad \xi^z = 1, \qquad \hat{\phi}^{\mathcal{A}} = -\mathcal{A}_z, \qquad \hat{\phi}^{P} = -P_z. \tag{3.41}$$

Using (3.36) we obtain

$$W^1 = B\left(E + \frac{E^{2\sigma+1}}{2\sigma+2} - P\right) - \frac{P_z P_t}{\alpha}, \qquad W^2 = B^2. \tag{3.42}$$

The action (2.12) is invariant under the transformation. Using Noether's theorem (3.20), the conserved density $W_2 = W^1$ and flux $F_2 = W^2 + L$ are given by

$$W_2 = B\left(E + \frac{E^{2\sigma+1}}{2\sigma+1} + P\right) - \frac{P_z P_t}{\alpha}, \tag{3.43}$$

$$F_2 = \frac{1}{2}(E^2 + B^2) + \frac{E^{2\sigma+2}}{(2\sigma+1)(2\sigma+2)} + \frac{1}{2\alpha}(P_t^2 - P^2) + EP. \tag{3.44}$$

The conservation law in this case is the electromagnetic momentum conservation equation.

The above energy and momentum conservation laws can be expressed more concisely in the form

$$\frac{\partial T^{\mu\nu}}{\partial x^\mu} = 0 \quad (\nu = 0, 1), \tag{3.45}$$

where we use the Einstein summation convention for repeated indices; $(x^0, x^1) = (t, z)$; and $T^{\mu\nu}$ is the energy–momentum tensor for the system, with components

$$T^{00} = W_1, \qquad T^{10} = F_1, \qquad T^{01} = W_2, \qquad T^{11} = F_2. \tag{3.46}$$

From field theory (e.g. [13,14]) $T^{\mu\nu}$ is given in terms of the Lagrangian density $\mathcal{L}$ by the formulae:

$$T^{\mu\nu} = g^{\nu\sigma}T^{\mu}_{\sigma}, \qquad T^{\mu}_{\sigma} = \frac{\partial \mathcal{L}}{\partial q^\alpha_\mu}\frac{\partial q^\alpha}{\partial x^\sigma} - \delta^\mu_\sigma \mathcal{L}, \tag{3.47}$$

where $(q^1, q^2) = (\mathcal{A}, P)$ are the canonical coordinates, and the metric tensor $g^{\mu\nu} = \mathrm{diag}(1, -1)$ is the Minkowski, flat space metric tensor.

3.2.3.3. Translation invariance of B (X_3). In this case $\xi^t = \xi^z = \hat{\phi}^P = 0$ and $\hat{\phi}^{\mathcal{A}} = z$. For this symmetry, the action (2.12) is not invariant. However

$$\hat{X}L = \left(z\frac{\partial}{\partial \mathcal{A}} + \frac{\partial}{\partial \mathcal{A}_z}\right)L = -\mathcal{A}_z, \tag{3.48}$$

and hence Boyer's form of Noether's theorem (3.18) applies with $\mathbf{A} = (0, -\mathcal{A})^{\mathrm{T}}$. The conserved density $W_3 = -W^1$ and flux $F_3 = -(W^2 - A^2)$ are given by

$$W_3 = z\left(E + \frac{E^{2\sigma+1}}{2\sigma+1} + P\right), \qquad F_3 = zB - \mathcal{A}. \tag{3.49}$$

3.2.3.4. Guage invariance (X_4). In this case $\xi^t = \xi^z = \hat{\phi}^P = 0$ and $\hat{\phi}^{\mathcal{A}} = 1$. The action (2.12) is invariant under the transformation. Noether's theorem (3.20) gives $W_4 = -W^1$ for the conserved density and $F_4 = -W^2$ for the conserved flux as:

$$W_4 = E + \frac{E^{2\sigma+1}}{2\sigma+1} + P, \quad F_4 = B. \tag{3.50}$$

The conservation equation in this case is Ampere's equation (2.2) which is one of the original basic equations of the model.

4. Similarity solutions

In this section, we obtain classical similarity solutions of the Maxwell–Lorentz system (2.7) and (2.8). These solutions involve four parameters, corresponding to the four Lie point symmetries discussed in Section 3.2. The most useful solutions are the traveling wave solutions associated with the space and time translation symmetries. The latter solutions are investigated in Section 5.

4.1. Classical similarity solutions

From (3.27), the general Lie point symmetry operator X admitted by the system (2.7) and (2.8) is

$$X = a_1\frac{\partial}{\partial t} + a_2\frac{\partial}{\partial z} + (a_3 z + a_4)\frac{\partial}{\partial \mathcal{A}}, \tag{4.1}$$

where $\{t, z, \mathcal{A}, P\}$ are the basic variables.

The classical similarity solutions of the system (2.7) and (2.8) are obtained by integrating the group trajectories (e.g. Section 3.1.1, [7,8,15]):

$$\frac{\mathrm{d}t}{\mathrm{d}\tau} = a_1, \qquad \frac{\mathrm{d}z}{\mathrm{d}\tau} = a_2, \qquad \frac{\mathrm{d}\mathcal{A}}{\mathrm{d}\tau} = a_3 z + a_4, \qquad \frac{\mathrm{d}P}{\mathrm{d}\tau} = 0, \tag{4.2}$$

where τ is a parameter along the trajectories. Integration of (4.2) yields the integrals:

$$z - st = J_1, \qquad \mathcal{A} - (\tfrac{1}{2}\delta z^2 + \nu z) = J_2, \qquad P = J_3 \tag{4.3}$$

for the group invariants $\{J_1, J_2, J_3\}$, where

$$s = \frac{a_2}{a_1}, \qquad \delta = \frac{a_3}{a_1}, \qquad \nu = \frac{a_4}{a_1} \tag{4.4}$$

(we implicitly assume $a_1 \neq 0$). From (4.4) it follows that the Maxwell system (2.7) and (2.8) possesses classical similarity solutions of the form:

$$\mathcal{A} = \tfrac{1}{2}\delta z^2 + \nu z + A(\xi), \qquad P = P(\xi), \tag{4.5}$$

where

$$\xi = z - st, \tag{4.6}$$

is the similarity variable, and $A(\xi)$ and $P(\xi)$ are functions of ξ obtained by substituting the solution ansatz (4.5) and (4.6) into (2.7) and (2.8).

From (2.6), the solutions for E and B have the form:

$$E = sA'(\xi), \qquad B = \delta z + \nu + A'(\xi). \tag{4.7}$$

The solutions for $P(\xi)$ and $A(\xi)$ depend on the traveling wave variable $\xi = z - st$, where s is the velocity of the traveling wave frame. From (4.7)

$$E - sB = -s(\nu + \delta z). \tag{4.8}$$

Noting that $\mathbf{E} = (E, 0, 0)^{\mathrm{T}}$, $\mathbf{B} = (0, B, 0)^{\mathrm{T}}$ and setting $\mathbf{u} = (0, 0, s)^{\mathrm{T}}$ for the velocity of the traveling wave frame, we find

$$\tilde{\mathbf{E}} = \gamma(\mathbf{E} + \mathbf{u} \times \mathbf{B}) = \gamma(0, 0, E - sB)^{\mathrm{T}} \tag{4.9}$$

for the electric field in the traveling wave frame, where γ is the Lorentz gamma. Thus, we may identify the right hand side of (4.8) with the electric field in the traveling wave frame.

Substituting the solution ansatz (4.5) and (4.6) into Ampere's law (2.7), and integrating with respect to ξ yields the integral:

$$\delta\xi + \frac{E}{s} - s\left(E + \frac{E^{2\sigma+1}}{2\sigma+1} + P\right) = c_1, \tag{4.10}$$

where c_1 is an integration constant. The Lorentz oscillator equation (2.8) becomes:

$$s^2 P''(\xi) + P = \alpha E. \tag{4.11}$$

Hence the system reduces to a second order ODE for P coupled with an algebraic equation relating P and E (we could of course also write the equations in terms of $A(\xi)$ and $P(\xi)$, using the fact that $E = sA'(\xi)$).

Eq. (4.10) can be solved for P in terms of E, yielding the equation:

$$P = g(E) + \frac{\delta\xi}{s}, \tag{4.12}$$

where

$$g(E) = \frac{E(1 - s^2)}{s^2} - \frac{E^{2\sigma+1}}{2\sigma+1} - \frac{c_1}{s}. \tag{4.13}$$

Using the result (4.12) for P in (4.11) yields a second order differential equation for $E(\xi)$ of the form:

$$s^2(g'(E)E_{\xi\xi} + g''(E)E_\xi^2) + g(E) - \alpha E + \frac{\delta\xi}{s} = 0. \tag{4.14}$$

Thus, the similarity solutions for the system can be obtained by integrating the non-linear, second order, ordinary differential equation (4.14) for $E = E(\xi)$.

Note that a second independent integral of the system (4.10) and (4.11) can be obtained by substituting the solution ansatz (4.5) and (4.6) into the energy conservation equation (3.35) for $j = 1$, where the conserved energy density $W_1 \equiv \mathcal{H}$, and energy flux F_1 are given in (3.39) and (3.40). This yields the energy conservation equation:

$$\frac{s^2 P_\xi^2 + P^2}{2\alpha} + \frac{E^2}{2} + \frac{E^{2\sigma+2}}{2\sigma+2} - \frac{1}{2}A_\xi^2 - \delta A = \tilde{\epsilon}, \tag{4.15}$$

where $\tilde{\epsilon}$ is the energy integration constant. One can also obtain the integral (4.15) by combining the derivative of (4.10) with (4.11).

5. Traveling wave solutions

In this section, we consider the class of traveling wave similarity solutions. These solutions correspond to the case $\delta = 0$ in (4.4). We first obtain the canonical Poisson bracket for the traveling wave solutions, and then use this bracket to obtain the non-canonical Poisson bracket using (E, p) as the variables, where E and $p = P_\xi$ are the electric field and canonical momentum, respectively. An analysis of the (E, p)-phase-space trajectories is used to determine the different types of traveling waves that can be obtained depending on the traveling wave speed s, α and the energy integration constant H_0 for the waves. This is followed by some illustrative examples.

5.1. Poisson brackets for the traveling waves

The basic differential equations for the system (4.10) and (4.11) may be cast in the Hamiltonian form:

$$\frac{\partial q}{\partial \xi} = \frac{\partial H_0}{\partial p}, \qquad \frac{\partial p}{\partial \xi} = -\frac{\partial H_0}{\partial q}, \tag{5.1}$$

where

$$q = P \quad \text{and} \quad p = P_\xi, \tag{5.2}$$

are the canonical variables and

$$H_0 = N\left(\frac{s^2 p^2 + q^2}{2\alpha} + \frac{E^2(s^2-1)}{2s^2} + \frac{E^{2\sigma+2}}{2\sigma+2}\right) \equiv N\tilde{\epsilon}, \tag{5.3}$$

is a re-scaled version of the energy integral (4.15) with normalization constant

$$N = \frac{\alpha}{s^2}. \tag{5.4}$$

In order to express the Hamiltonian H_0 in terms of the canonical variables it is necessary to invert the relation (4.12) for $\delta = 0$, i.e. to solve the equation:

$$q = \frac{E(1-s^2)}{s^2} - \frac{E^{2\sigma+1}}{2\sigma+1} - \frac{c_1}{s} \tag{5.5}$$

for E as a function of q. Since there are multiple roots of (5.5) for $E = E(q)$, it is in general simpler to use a non-canonical Poisson bracket description of the equations, in which (E, p) are the non-canonical phase-space coordinates.

In the canonical Poisson bracket description of Hamilton's equation (5.1), the equations are written in the form $\eta_\xi = \{\eta, H_0\}_c$, where $\eta = (q, p)^{\mathrm{T}}$ are the canonical variables, and $\xi = z - st$ is the traveling wave variable. The canonical Poisson bracket $\{F, G\}_c$ has the form:

$$\{F, G\}_c = \frac{\partial F}{\partial q}\frac{\partial G}{\partial p} - \frac{\partial F}{\partial p}\frac{\partial G}{\partial q} \equiv (F_q, F_p)\cdot \mathbf{J}\cdot (G_q, G_p)^{\mathrm{T}}, \tag{5.6}$$

where

$$\mathbf{J} = \begin{pmatrix} 0 & 1 \\ -1 & 0 \end{pmatrix}, \tag{5.7}$$

is the canonical symplectic matrix.

If one uses the non-canonical variables (E, p) Hamilton's equations for the system may be written in the Poisson bracket form:

$$\tilde{\eta}_\xi = \{\tilde{\eta}, \tilde{H}_0\} \quad \text{where } \tilde{\eta} = (E, p)^{\mathrm{T}}. \tag{5.8}$$

Here, the non-canonical Poisson bracket $\{\tilde{F}, \tilde{G}\}$ is

$$\{\tilde{F}, \tilde{G}\} = E_q\left(\frac{\partial \tilde{F}}{\partial E}\frac{\partial \tilde{G}}{\partial p} - \frac{\partial \tilde{F}}{\partial p}\frac{\partial \tilde{G}}{\partial E}\right) \equiv \nabla_{\tilde{\eta}}\tilde{F}^{\mathrm{T}}\cdot\tilde{\mathbf{J}}\cdot\nabla_{\tilde{\eta}}\tilde{G}, \tag{5.9}$$

where

$$\tilde{\mathbf{J}} = \begin{pmatrix} 0 & E_q \\ -E_q & 0 \end{pmatrix}, \tag{5.10}$$

is the symplectic matrix operator for the non-canonical bracket. From (5.5) we find

$$E_q = \frac{1}{y_c - E^{2\sigma}} \quad \text{where } y_c = \frac{1-s^2}{s^2}. \tag{5.11}$$

Note that $\tilde{F}(E, p) = F(q, p)$ and $\{\tilde{F}, \tilde{G}\} = \{F, G\}_c$ define the non-canonical bracket in terms of the canonical bracket.

It remains to check the skew-symmetry and the Jacobi identity for the non-canonical bracket (5.9). The skew-symmetry of the bracket follows from the skew-symmetry of $\tilde{\mathbf{J}}$ (i.e. $\tilde{\mathbf{J}}^{\mathrm{T}} = -\tilde{\mathbf{J}}$). From [8, p. 395, Eq. (6.15)], the Jacobi identity is satisfied if

$$\mathcal{I}(i, j, k) = \sum_{\ell=1}^{2} \tilde{J}^{i\ell}\partial_\ell \tilde{J}^{jk} + \tilde{J}^{k\ell}\partial_\ell \tilde{J}^{ij} + \tilde{J}^{j\ell}\partial_\ell \tilde{J}^{ki} = 0, \quad i, j, k = 1, 2, \tag{5.12}$$

where $\partial_\ell = \partial/\partial x^\ell$ and $(x^1, x^2) = (E, p) = \tilde{\eta}^{\mathrm{T}}$. Noting that $\tilde{J}^{ij}$ is independent of p, and evaluating the derivatives in (5.12) we find that (5.12) is satisfied provided $y_c - E^{2\sigma} \neq 0$. Hence the Jacobi identity is satisfied for the non-canonical Poisson bracket, provided we avoid the singular manifold $y_c - E^{2\sigma} = 0$, where $|E_q| \to \infty$ and $|\mathrm{d}E_q/\mathrm{d}E| \to \infty$.

The above analysis shows that the (E, p)-phase plane for $0 < s^2 < 1$ (i.e. $y_c > 0$) splits into three separate regions: (i) $E < -E_c$, (ii) $|E| < E_c$ and (iii) $E > E_c$, where

$$E_c = \left(\frac{1-s^2}{s^2}\right)^{1/2\sigma}. \tag{5.13}$$

Thus, the Hamiltonian dynamics may be thought of as occurring on three separate distinct manifolds, or regions which are separated by the singular lines $E = \pm E_c$ in the (E, p)-phase plane.

5.2. Phase-space trajectories and critical point analysis

Hamilton's equation (5.8) for the evolution of $\tilde{\eta} = (E, p)^{\mathrm{T}}$ may be written in the form:

$$\frac{\mathrm{d}E}{\mathrm{d}\xi} = -\frac{p}{E^{2\sigma} - y_c}, \qquad \frac{\mathrm{d}p}{\mathrm{d}\xi} = \frac{1}{s^2}\left((\alpha - y_c)E + \frac{E^{2\sigma+1}}{2\sigma+1} + \frac{c_1}{s}\right). \tag{5.14}$$

To further investigate the phase-space trajectories (5.14) we restrict our analysis to the case of a cubic Kerr non-linearity ($\sigma = 1$) and assume $c_1 = 0$.

5.2.1. Case $\sigma = 1$ and $c_1 = 0$

In this case the phase-space trajectories (5.14) reduce to the equation system:

$$\frac{\mathrm{d}E}{\mathrm{d}\xi} = -\frac{p}{E^2 - y_c}, \qquad \frac{\mathrm{d}p}{\mathrm{d}\xi} = \frac{E(E^2 - y_e)}{3s^2}, \tag{5.15}$$

where

$$y_e = 3(y_c - \alpha), \qquad y_c = \frac{1 - s^2}{s^2}. \tag{5.16}$$

The autonomous system (5.15) can also be written in the form:

$$\frac{\mathrm{d}p}{\mathrm{d}\tau} = -\frac{E(E^2 - y_e)(E^2 - y_c)}{3s^2} \equiv G(E), \qquad \frac{\mathrm{d}E}{\mathrm{d}\tau} = p, \tag{5.17}$$

where τ is a parameter along the trajectories. Note that in general, $|E_\xi| \to \infty$ as $E \to \pm E_c$, where $E_c = y_c^{1/2}$ (unless $p \to 0$ also in this limit). Also note that E_ξ changes sign as we cross $E = \pm E_c$.

From (5.3) and (5.5)

$$H_0 = N\tilde{\epsilon} = N\left(\frac{s^2p^2 + E^2(y_c - E^2/3)^2}{2\alpha} - \frac{E^2 y_c}{2} + \frac{E^4}{4}\right), \tag{5.18}$$

is the general integral of (5.17). Thus, the trajectories (5.17) in the (E, p)-phase plane can be obtained by plotting the contours of H_0.

The critical points of the dynamical system (5.17) occur at the points where $\mathrm{d}p/\mathrm{d}\tau = \mathrm{d}E/\mathrm{d}\tau = 0$ simultaneously. The critical points in the (E, p) plane are located at:

$$(\pm E_c, 0), \qquad (\pm E_e, 0) \quad \text{and} \quad (0, 0), \tag{5.19}$$

where

$$E_c = y_c^{1/2}, \qquad E_e = y_e^{1/2}. \tag{5.20}$$

Linearization of (5.17) about the critical points (5.19) yields the equations:

$$\frac{\mathrm{d}}{\mathrm{d}\tau}\begin{pmatrix}\delta p \\ \delta E\end{pmatrix} = \begin{pmatrix}0 & G'(E_{\mathrm{cr}}) \\ 1 & 0\end{pmatrix}\begin{pmatrix}\delta p \\ \delta E\end{pmatrix} \equiv \mathbf{A}\begin{pmatrix}\delta p \\ \delta E\end{pmatrix}, \tag{5.21}$$

where E_{cr} denotes a value of E at a critical point, and $G'(E) \equiv \mathrm{d}G/\mathrm{d}E$.

Table 1
Properties of the critical points in the (E, p)-phase plane for the traveling wave solutions of the Maxwell–Lorentz system (2.1)–(2.4) (the (E, p) phase plane trajectories are given in (5.17))

Case	Velocity range	$(\pm E_e, 0)$	$(\pm E_c, 0)$	$(0, 0)$	Comment
(a)	$0 < \|s\| < s_1$	Center	Saddle	Center	$E_e > E_c > 0$
(b)	$s_1 < \|s\| < s_2$	Saddle	Center	Center	$E_c > E_e > 0$
(c)	$s_2 < \|s\| < 1$	–	Center	Saddle	$E_c > 0, E_e^2 < 0$
(d)	$\|s\| > 1$	–	–	Center	$E_c^2 < 0, E_e^2 < 0$

Searching for solutions $(\delta p, \delta E)^{\mathrm{T}} = \mathbf{R}\exp(\lambda\tau)$ yields the eigen-equation system:

$$(\mathbf{A} - \lambda\mathbf{I})\mathbf{R} \equiv \begin{pmatrix} -\lambda & G'(E_{\mathrm{cr}}) \\ 1 & -\lambda \end{pmatrix} \begin{pmatrix} r_1 \\ r_2 \end{pmatrix} = \begin{pmatrix} 0 \\ 0 \end{pmatrix}, \tag{5.22}$$

where $\mathbf{R} = (r_1, r_2)^{\mathrm{T}}$ is the right eigenvector of the matrix $\mathbf{A}$ corresponding to the eigenvalue λ. Eq. (5.22) has a non-trivial solution for $\mathbf{R}$ provided λ satisfies the eigenvalue equation:

$$\det(\mathbf{A} - \lambda\mathbf{I}) = \lambda^2 - G'(E_{\mathrm{cr}}) = 0, \tag{5.23}$$

and $\mathbf{R} = (\lambda, 1)^{\mathrm{T}} r_2$ is the corresponding eigenvector, where r_2 is an arbitrary constant. Evaluating $G'(E_{\mathrm{cr}})$, we find that $\lambda = \pm\lambda_0$, $\lambda = \pm\lambda_c$, or $\lambda = \pm\lambda_e$ corresponding to the points $(0, 0)$, $(\pm E_c, 0)$ and $(\pm E_e, 0)$, where

$$\lambda_0^2 = \frac{[s^2(1+\alpha) - 1](1 - s^2)}{s^6}, \qquad \lambda_c^2 = \frac{4(1 - s^2)[1 - (1 + 3\alpha/2)s^2]}{s^6},$$
$$\lambda_e^2 = \frac{4[1 - s^2(1+\alpha)][(1 + 3\alpha/2)s^2 - 1]}{s^6}. \tag{5.24}$$

Inspection of (5.24) shows that the signs of λ_0^2, λ_c^2 and λ_e^2 can change at the characteristic speeds:

$$s_1 = (1 + \tfrac{1}{2}3\alpha)^{-1/2}, \qquad s_2 = (1+\alpha)^{-1/2}, \qquad s_3 = 1, \tag{5.25}$$

where $0 < s_1 < s_2 < s_3 = 1$. The nature of the critical points (5.19) (i.e., whether the critical point is a saddle or a center or something more complicated) depends on the speed of the traveling wave and the value of α. In addition, the energy integration constant ϵ has a specific value for the trajectories that pass through the critical point, in the case that the critical point is a saddle. A summary of the nature of the different critical points is given in Table 1.

The above information is sufficient to sketch the phase trajectories in the (E, p)-phase plane, in the four speed regimes: (a) $0 < |s| < s_1$, (b) $s_1 < |s| < s_2$, (c) $s_2 < |s| < 1$, and (d) $|s| > 1$. The trajectories can be obtained by plotting the contours of the Hamiltonian $H_0 = \tilde{H}_0(E, p)$ in (5.18) or by numerically integrating the differential equations (5.17). Alternatively, one can obtain an explicit representation for the trajectories in the form $p = p(E)$, by solving (5.18) for p^2:

$$p^2 = \frac{1}{9s^2}\left[\epsilon - \frac{9\alpha}{2}(E^4 - 2y_c E^2) - E^2(E^2 - 3y_c)^2\right] \equiv \frac{\Phi(y)}{9s^2}, \tag{5.26}$$

where

$$\epsilon = 18\alpha\tilde{\epsilon} \equiv 18s^2 H_0, \qquad y = E^2 \tag{5.27}$$

(note ϵ is a re-scaled version of the energy integration constant H_0). In the present example with $c_1 = 0$ and $\sigma = 1$, p^2 is a cubic polynomial in $y = E^2$. In the more general case where $c_1 \neq 0$ this is not true. The polynomial $\Phi(y)$ in (5.26) is

$$\Phi(y) = \epsilon - (y^3 + \beta_4 y^2 + \beta_2 y), \tag{5.28}$$

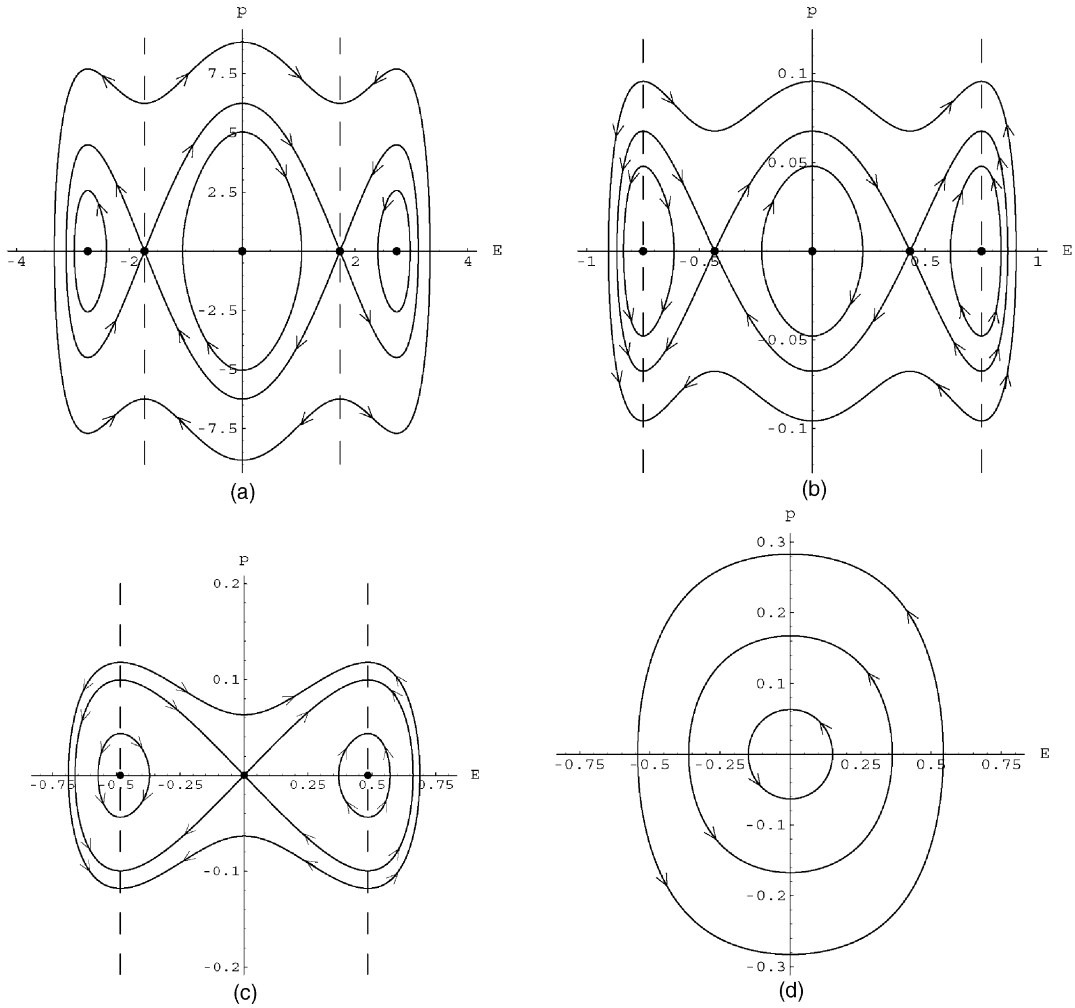

Fig. 1. Phase trajectories (5.26), or the contours of the Hamiltonian H_0 (5.18) in the (E, p)-phase plane for the traveling wave solutions of the Maxwell–Lorentz system. The parameters $c_1 = 0$ and $\alpha = 0.5$. The four cases are: (a) $s = 0.5$, (b) $s = 0.8$, (c) $s = 0.9$ and (d) $s = 1.2$, corresponding to the four different speed regimes in Table 1.

where

$$\beta_4 = \frac{9\alpha}{2} - 6y_c, \qquad \beta_2 = 9y_c(y_c - \alpha), \qquad y_c = \frac{1 - s^2}{s^2}. \tag{5.29}$$

From (5.5) $p = q_\xi = (y_c - y)E_\xi$, and hence the phase plane trajectory (5.26) is equivalent to the first order differential equation

$$\left(\frac{\mathrm{d}y}{\mathrm{d}\xi}\right)^2 = \frac{4y\Phi(y)}{9s^2(y - y_c)^2} \tag{5.30}$$

for y as a function of ξ.

Representative phase-space trajectories (5.26) in the (E, p)-phase plane are given in Fig. 1(a)–(d), which correspond to the different cases in Table 1. The parameters used in Fig. 1(a), $s = 0.5$ and $\alpha = 0.5$ and $c_1 = 0$,

corresponds to the velocity regime $0 < |s| < s_1$. In this regime $E_e > E_c > 0$. The different orbits correspond to different values of the energy integration constant ϵ in (5.26). On the vertical dashed lines at $E = \pm E_c$, $|E_\xi| \to \infty$, and E_ξ changes sign across $E = \pm E_c$. The arrows correspond to the direction of increasing ξ. Inside the heteroclinic orbit joining the saddles at $(\pm E_c, 0)$ there are closed orbits corresponding to smooth, periodic traveling waves of the Maxwell–Lorentz system (2.1)–(2.4). Note in general that $|E_\xi| \to \infty$ for the solution trajectories that intersect with the curves $E = \pm E_c$, except for the special separatrix solution which passes smoothly through the saddle points at $(\pm E_c, 0)$. For $|E| > E_c$, there are periodic orbits inside the separatrix which circle about the centers at $(\pm E_e, 0)$. These solutions give rise to smooth, periodic traveling waves. Trajectories outside the separatrix, have the property $|E_\xi| \to \infty$ as $E \to \pm E_c$. Note from (5.15) that the tangent vector to the curves (E_ξ, p_ξ) reverse across the vertical lines $E = \pm E_c$. The arrows on the curves show the direction of increasing ξ, as determined from the tangent vector (E_ξ, p_ξ) from (5.15).

We now consider more precisely the character of the separatrix in Fig. 1(a) which passes smoothly through the saddle point singularities at $(\pm E_c, 0)$. This solution is called the critical solution by analogy with the transonic solution in stellar wind theory, where the wind passes smoothly through the sonic critical point from subsonic to supersonic flow [26]. The phase-space trajectories correspond to solutions of the first order differential equation (5.30) for $y(\xi)$. For an appropriate choice of ϵ, $\Phi(y)$ has a double zero at $y = y_c$, and the factor of $(y - y_c)^2$ in the denominator of (5.30) cancels with a corresponding factor of $(y - y_c)^2$ of $\Phi(y)$ in the numerator.

More generally, we can look for other special solutions of (5.30) for which $\Phi(y)$ has a double zero at $y = y_r$ say, i.e. $\Phi(y_r) = \Phi'(y_r) = 0$ simultaneously at $y = y_r$. Differentiating (5.28) yields

$$\Phi'(y) = -3(y - y_c)(y - y_e), \tag{5.31}$$

where $y_e = 3(y_c - \alpha)$ and $y_c = (1 - s^2)/s^2$ (see (5.16)). Thus, $y = y_c$ and $y = y_e$ are both double roots of $\Phi(y) = 0$ for appropriate choices of the energy integration constant ϵ. The first possibility $y = y_c$ corresponds to the critical solution. The second possibility $y = y_e$ corresponds to the heteroclinic orbit in Fig. 1(b), and gives rise to a kink-type solution. Below we consider in more detail the critical solution case.

(i) *The critical solution*

The conditions $\Phi'(y_c) = 0$ and $\Phi(y_c) = 0$ are satisfied by choosing

$$\epsilon = \epsilon_{\rm cr} = y_c^2 y_d \quad \text{where} \quad y_d = \tfrac{1}{2}(4y_c - 9\alpha). \tag{5.32}$$

In this case

$$\Phi(y) = \Phi^{(c)}(y) = -(y - y_c)^2(y - y_d). \tag{5.33}$$

Thus, the equation of the separatrix in Fig. 1(a) is $p^2 = \Phi^{(c)}(y)/9s^2$, where $y = E^2$. Note that $p = 0$ at $y = y_c$ $(E = \pm E_c)$, and at $y = y_d$ $(E = \pm E_d$, where $E_d = y_d^{1/2})$. In order for E_d to be real requires that $y_d > 0$. This latter condition requires that the wave speed s be restricted to the range $0 < |s| < (1 + 9\alpha/8)^{-1/2}$. The differential equation (5.30) reduces to:

$$\frac{{\rm d}y}{{\rm d}\xi} = \pm\frac{2}{3s}[y(y_d - y)]^{1/2}. \tag{5.34}$$

Note that the $(y - y_c)^2$ factor in $\Phi^{(c)}(y)$ cancels with the $(y - y_c)^2$ factor in the denominator in (5.30). The solution of (5.34) is

$$y = y_d \sin^2\left(\frac{\xi - \xi_0}{3s}\right), \tag{5.35}$$

where ξ_0 is an integration constant. The corresponding solution for E is

$$E = \pm y_d^{1/2} \sin\left(\frac{\xi - \xi_0}{3s}\right). \tag{5.36}$$

For the solution for E to be real requires that $y_d > 0$. Since

$$y_d = \frac{4}{s^2}\left[1 - \left(1 + \frac{9\alpha}{8}\right)s^2\right], \tag{5.37}$$

it is necessary to choose $0 < |s| < (1 + 9\alpha/8)^{-1/2}$ in order to ensure that E is real. The solution is a smooth, periodic traveling wave. It is straightforward to show that the electric field amplitude $E_d = y_d^{1/2}$, and the Hamiltonian integral $H_0 = y_c^2 y_d/18s^2$ both tend to zero as $|s| \to (1+9\alpha/8)^{-1/2}$ and that both E_d and H_0 are unbounded in the limit as $|s| \to 0$.

Fig. 1(b) shows a typical phase-space plot of the trajectories (5.26) for the speed regime $s_1 < |s| < s_2$ of Table 1. In this regime $E_c > E_e$, and heteroclinic orbits connect the two saddles at $(-E_e, 0)$ and $(E_e, 0)$, where $E_e = y_e^{1/2}$. The periodic orbits which circle the origin $(0, 0)$ in the (E, p) plane correspond to smooth, periodic traveling wave solutions. The solutions with $|E| > E_c$ develop infinite electric field gradients $|E_\xi|$ at $E = \pm E_c$. Below, we consider in more detail the heteroclinic orbits connecting the saddles at $(\pm E_e, 0)$.

(ii) *The heteroclinic orbit*

From (5.31), we know that $\Phi'(y_e) = 0$. By choosing

$$\epsilon = \epsilon_h = \frac{3\alpha}{2} y_e^2 \quad \text{or} \quad H_0 = \frac{(3\alpha/2)y_e^2}{18s^2}, \tag{5.38}$$

ensures that $\Phi(y_e) = 0$ also. In this case $y = y_e$ is a double root of $\Phi(y) = 0$. Using this value of ϵ, we obtain

$$\Phi^{(h)}(y) \equiv \Phi(y) = (y - y_e)^2(\tfrac{1}{2}3\alpha - y), \tag{5.39}$$

as the form of $\Phi(y)$ for $\epsilon = \epsilon_h$. The corresponding phase-space trajectory in the (E, p) plane (5.26) has the form: $p^2 = \Phi^{(h)}(y)/9s^2$, where $y = E^2$. This trajectory is the heteroclinic orbit in Fig. 1(b).

From (5.30) the corresponding differential equation for $y = y(\xi)$ reduces to:

$$\frac{\mathrm{d}y}{\mathrm{d}\xi} = \pm\frac{2(y - y_e)}{3s(y - y_c)}\left[y\left(\frac{3\alpha}{2} - y\right)\right]^{1/2}. \tag{5.40}$$

Note that (5.40) has a singularity at $y = y_c$. At $y = y_e$, $y'(\xi) = 0$ and $p = 0$. This point corresponds to the saddle points at $(\pm E_e, 0)$ in the (E, p) plane. The differential equation (5.40) can be integrated to obtain an implicit, exact solution for $y = y(\xi)$ in the form:

$$\xi = \sigma s\left[\frac{1}{\tau_e}\ln\left|\left(\frac{\tau + \tau_e}{\tau - \tau_e}\right)\right| + \frac{3\theta}{2}\right], \tag{5.41}$$

where $\sigma = \pm 1$ and the integration constant in (5.41) has been set equal to zero. The functions $\tau = \tau(y)$ and $\theta = \theta(y)$, the constant τ_e and E are given by

$$y = \frac{3\alpha}{2}\sin^2\left(\frac{\theta}{2}\right), \qquad E = \left(\frac{3\alpha}{2}\right)^{1/2}\sin\left(\frac{\theta}{2}\right), \qquad \tau = \tan\left(\frac{\theta}{2}\right) = \pm\left(\frac{y}{3\alpha/2 - y}\right)^{1/2},$$
$$\tau_e = \tan\left(\frac{\theta_e}{2}\right) = \left(\frac{y_e}{3\alpha/2 - y_e}\right)^{1/2}. \tag{5.42}$$

If we restrict the range of θ in (5.41) and (5.42) to $|\theta| < \theta_e$, then $y < y_e$. For the case where the sign function $\sigma = 1$ in (5.41), we find that $E \to -y_e^{1/2}$ as $\xi \to -\infty$ and $E \to y_e^{1/2}$ as $\xi \to \infty$. This is a kink-type solution, which is illustrated in the next subsection.

The critical solution in Fig. 1(a) plays the role of a separatrix in the speed regime $0 < |s| < s_1$. However, for $s_1 < |s| < (1+9\alpha/8)^{-1/2}$, the critical solution corresponds to a smooth periodic orbit about the origin, which lies inside the separatrix, in Fig. 1(b), and the diameter of the orbit shrinks to zero as $|s| \to (1+9\alpha/8)^{-1/2}$. This is consistent with the formulae (5.32) and (5.38) for $\epsilon_{\rm cr}$ and $\epsilon_{\rm h}$, which represent the contour heights of the critical and heteroclinic orbits in the (E, p) plane. In particular

$$\epsilon_{\rm h} = \epsilon_{\rm cr} + 4(\tfrac{3\alpha}{2} - y_c)^3. \tag{5.43}$$

Thus, $\epsilon_{\rm cr} > \epsilon_{\rm h}$ in the velocity range $0 < |s| < s_1$, $\epsilon_{\rm h} = \epsilon_{\rm cr}$ at $s = s_1$ and $\epsilon_{\rm h} > \epsilon_{\rm cr}$ for $s_1 < |s| < s_2$.

Fig. 1(c) shows the phase plane trajectories in the velocity regime $s_2 < |s| < 1$. In this regime, there are no smooth periodic traveling wave solutions, since all solutions unavoidably intersect the singular lines at $E = \pm E_c$, where $|E_\xi| \to \infty$. The separatrix orbit through the origin is given by $p^2 = \Phi^{(0)}(y)/9s^2$, where $\Phi^{(0)}(y)$ is the form of $\Phi(y)$ obtained with $\epsilon = 0$.

Fig. 1(d) illustrates the phase trajectories for $|s| > 1$. In this regime, there are periodic, ellipse like orbits about the origin in the (E, p) plane, which correspond to smooth periodic traveling waves.

5.3. Illustrative examples

For the traveling wave solutions (4.10) and (4.11), with $\delta = c_1 = 0$, and cubic Kerr non-linearity, the displacement current $D = E + P + E^3/3$, magnetic induction B and polarization P are given in terms of E by the formulae:

$$B = \nu + \frac{E}{s}, \qquad D = \frac{E}{s^2}, \qquad P = E\left(y_c - \frac{E^3}{3}\right), \tag{5.44}$$

where ν is a constant. Without loss of generality, we set $\nu = 0$ in the examples below.

Fig. 2 illustrates the critical solution $E = E_d \sin(\xi/3s)$ of (5.36) and (5.44) for the case $\nu = 0$, $\alpha = s = 0.5$. Panel (a) shows the variation of E, B, P and D as a function of the traveling wave variable $\xi = z - st$. The solutions for D and B are re-scaled versions of the profile for E ($D = E/s^2$ and $B = E/s$). The solution for P from (5.35) is a cubic in E and has a more complicated form. The trajectory in the (E, p)-phase plane is the critical solution or separatrix in Fig. 1(a). The critical solution trajectory passes smoothly through the critical points at $(\pm E_c, 0)$, and visits the three separate disjoint regions: $|E| < E_c$; $E > E_c$ and $E < -E_c$ in its periodic orbit. Panel (b) in Fig. 2 illustrates the same trajectory in the (q, p)-phase plane, where $q = P$ and $p = P_\xi$ are the canonical variables. The critical points in panel (b) are all center critical points. The phase plane trajectory starts on the outer ellipse at A ($\xi = 0$), and proceeds in a clockwise fashion to visit all three ellipses, until it ends up back at point A. Each ellipse

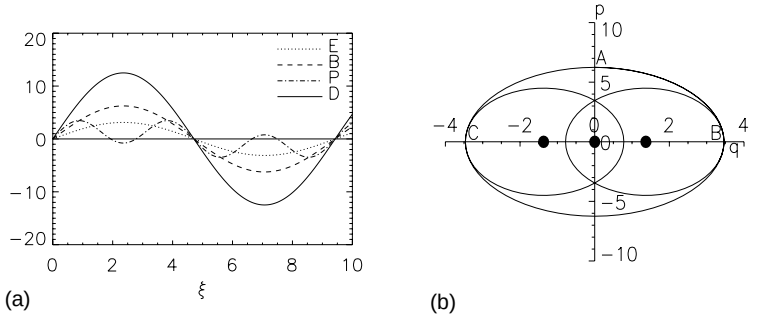

Fig. 2. (a) The variation of E, B, P and D for the critical solution $E = E_d \sin(\xi/3s)$ given in (5.36) and (5.44) with $\nu = 0$, and (b) the (q, p)-phase plane trajectory. The parameters are $\alpha = 0.5$ and $s = 0.5$.

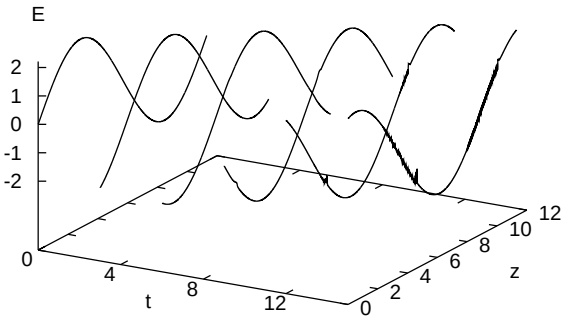

Fig. 3. The sinusoidal, critical solution (5.36) perturbed by 0.01 $\sin(z/6s)$ at time $t = 0$, for the case $\alpha = 0.5$ and $s = 0.6$. Note the formation of two shocks in the electric field. This results in instability at late times.

represents a different Hamiltonian branch, corresponding to the three solutions of (5.5) for $E = E(q)$ for the case $\sigma = 1$ and $c_1 = 0$.

The critical solution described in (5.36) and (5.44) has a sinusoidal solution for the electric field. We have used this exact solution of the vector Maxwell equations as a check on our numerical code. The code follows the exact solution as far in time as we have calculated ($t = 1000$). As a numerical test of the stability of the solution (5.36), we have added a small perturbation to the exact sinusoidal solution for E at time $t = 0$ of the form $0.01 \sin(z/6s)$ for the case $\alpha = 0.5$ and $s = 0.6$. The results of the numerical simulations are presented in Fig. 3. The figure shows that the sinusoidal solution is unstable for the given initial perturbation. The instability manifests itself by shock formation on the steep parts of the sinusoidal solution.

Fig. 4 illustrates the kink solution (5.41), (5.42) and (5.44) for the case $\alpha = 0.5$, $s = 0.8$ and $\nu = 0$. Panel (a) shows the profiles of E, B, P and D as functions of ξ, which consist of monotonic increasing, and odd functions of ξ. In particular, as noted in (5.42), etc. $E \to -y_e^{1/2} = -0.433$ as $\xi \to -\infty$ and $E \to y_e^{1/2}$ as $\xi \to \infty$. Panel (b) shows that the solution corresponds to the heteroclinic orbit connecting the two saddle points in the (q, p)-phase plane.

The kink solution is given by an implicit formula which makes it rather complicated to investigate its stability. Therefore, we conducted direct numerical simulations to illustrate the kink solution and to study its stability. By choosing $E(z, 0) = A_{\text{kink}} \tanh((z - z_0)/w)$ we start the simulations with an initial condition which is a fairly good approximation to the solution, both near $\xi = 0$, and for $|\xi| \to \infty$. This initial data can be thought of as a

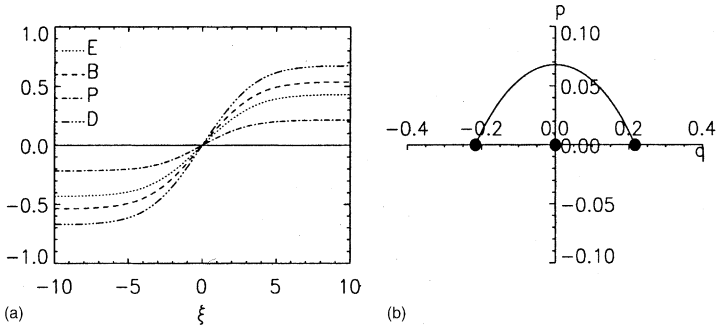

Fig. 4. Illustrates the kink solution described in (5.41), (5.42) and (5.44) for the case $\alpha = 0.5$, $s = 0.8$ and $\nu = 0$. Panel (a) shows the variation of E, B, P and D as functions of the traveling wave variable ξ. Panel (b) shows the solution corresponds to the heteroclinic orbit in the (q, p)-phase plane.

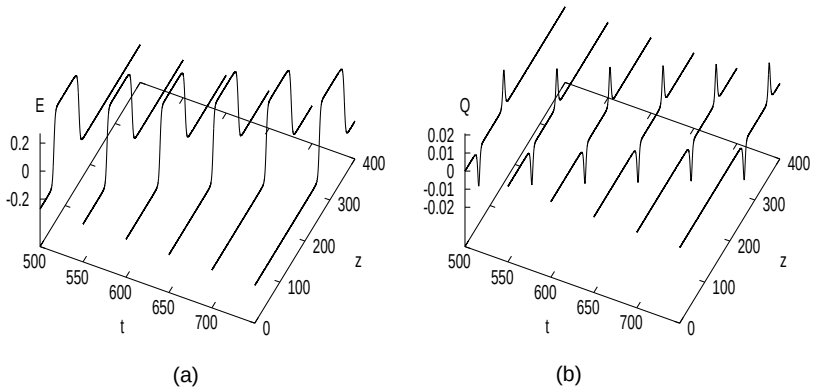

Fig. 5. A travelling kink and anti-kink wave, forming a square like pulse, using the parameter values $\alpha = 0.5$, $\sigma = 1$, $s = 0.81$. Panel (a) shows the E-field and (b) shows $Q = P_t$. The initial data are $A_{\text{kink}} = 0.269209$ and $w = 5.46321$.

perturbation of the exact kink solution, and serves as a test of the exact solution. The amplitude A_{kink} and width w are determined from the conservation of energy along the heteroclinic orbit connecting the two hyperbolic critical points. That is, $H_0(q = \alpha\sqrt{3(y_c - \alpha)}, p = 0) = H_0(q = 0, p_{\max})$. In other words, we match the approximate tanh -kink solution to the analytical one. It is also clear that when $E(z, 0)$ is fixed, the initial data for $B(z, 0)$ and $P(z, 0)$ can be calculated. Fig. 5(a) shows a kink and an anti-kink travelling in the same direction. The reason for presenting a kink anti-kink pair is due to our use of periodic boundary conditions in the numerical scheme. Only pairs of kinks and anti-kinks can satisfy these boundary conditions. Initially the kinks adjust their shape to the exact solution by shedding off linear radiation waves (not shown in Fig. 5). After a transient period the kinks attain the shape given by the analytical solution. In addition, for short periods of time we have added a space dependent damping term in the equation for P which we use to damp out the linear radiation away from the kinks. Fig. 5(a) shows the kinks propagating in a frictionless media given in Eqs. (2.1)–(2.4) after the transient period and after damping out radiation waves. Fig. 5(b) depicts the variable $Q = P_t$ as function of space and time. This variable has been introduced in order to write Eqs. (2.1)–(2.4) as a set of four first order differential equations, suitable for numerical solution.

Eqs. (2.1)–(2.4) have been solved numerically using fourth order accurate spatial central differences (five-point formula) [5]. The resulting first order system of ordinary differential equations was then solved using the DVERK Runge–Kutta algorithm based on Verner's fifth and sixth order formulas [6]. For $1 + 1$ dimensional problems we find this approach easy to implement, providing an accurate as well as robust method for numerical integration.

In order to investigate the robustness of the kinks we have conducted kink anti-kink collision experiments as shown in Fig. 6. The figure shows the spatial profiles of $E(z, t)$, $B(z, t)$, $P(z, t)$ and $Q(z, t) = P_t(z, t)$ at different time instants. The two pulses approaching each other at time $t = 0$ from opposite directions pass through each other, and approximately preserve their initial form provided the amplitude of the pulses are not too large. A small amount of radiation after the collision is observed indicating that the kinks (anti-kinks) are not solitons but merely solitary waves or quasi-solitons.

5.3.1. Traveling waves for $0 < |s| < s_1$ *and* $|s| > 1$

The ODE (5.40), which originally arose from analysis of the heteroclinic solution in the speed regime $s_1 < |s| < s_2$, can also be used outside this velocity regime. In fact, its solutions describe smooth periodic traveling waves in the speed regimes $0 < |s| < s_1$ and $|s| > 1$. It also describes solutions in which $|E_\xi| \to \infty$ as $E \to \pm E_c$ if $s_2 < |s| < 1$.

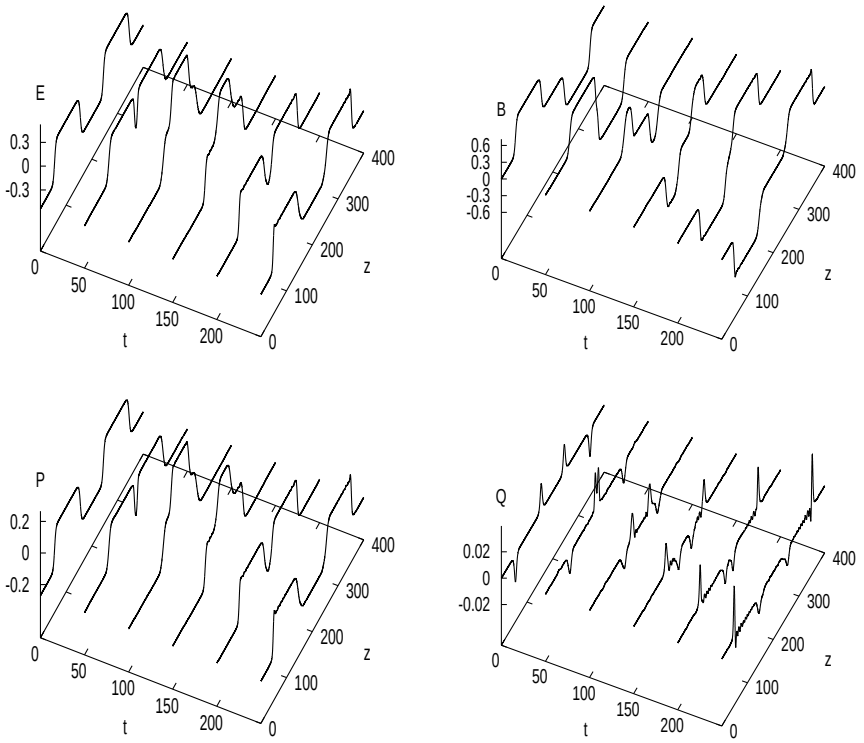

Fig. 6. Collision between two square like pulses. Parameter values $\alpha = 0.5$, $\sigma = 1$, $s = \pm 0.81$; $Q = P_t$.

In the above speed regime, the ODE (5.40) can be integrated to yield the solution:

$$\xi = s\left[3\tan^{-1}(\tau) - \frac{2}{\tau_0}\tan^{-1}\left(\frac{\tau}{\tau_0}\right)\right], \tag{5.45}$$

where

$$\tau = \tan\phi = \pm\left(\frac{y}{3\alpha/2 - y}\right)^{1/2}, \qquad \tau_0 = \left(\frac{\alpha - y_c}{3\alpha/2 - y_c}\right)^{1/2}, \tag{5.46}$$

and the parameters are ordered so that $0 < 3\alpha/2 < y_c < y_e$. A sketch of y_ξ^2 versus y from (5.40) shows that there are smooth periodic traveling waves for $0 < y < 3\alpha/2$. The electric field in the wave is given by

$$E = (\tfrac{1}{2}3\alpha)^{1/2}\sin\phi \tag{5.47}$$

(note $\theta = 2\phi$ in (5.42)). The solution (5.45) is strictly only defined for $|\phi| < \pi/2$, due to the multi-valued character of $\tan^{-1}(x)$. Taking the above ϕ-range to correspond to half a period of the wave, one can define the extension $\xi^{(E)}(\phi)$ of $\xi(\phi)$ by the equation

$$\xi^{(E)}(\phi) = \xi(\phi - n\pi) + \tfrac{1}{2}(n)T_\xi \quad \text{if } \phi \in [(n - \tfrac{1}{2})\pi, (n + \tfrac{1}{2})\pi], \tag{5.48}$$

where n is an integer, and

$$T_\xi = 2\pi s\left(3 - \frac{2}{\tau_0}\right) \equiv 2\pi s\left[3 - 2\left(\frac{1 - s^2(1 + 3\alpha/2)}{1 - s^2(1 + \alpha)}\right)^{1/2}\right], \tag{5.49}$$

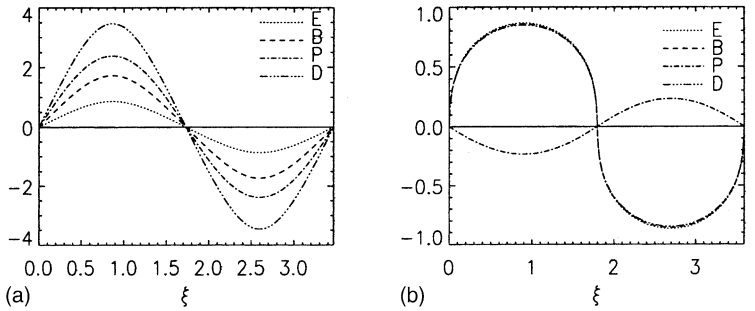

Fig. 7. Profiles of E, B, P and D as functions of ξ for the traveling wave solution (5.45)–(5.49) for the cases (a) $s = 0.5$ and (b) $s = 1.01$. The parameter $\alpha = 0.5$.

is the spatial period of the wave. Eq. (5.49) shows that the period of the wave depends on s, with $T_\xi \approx 2\pi s$ as $s \to 0$ and $T_\xi \approx 6\pi s$ as $s \to (1 + 3\alpha/2)^{-1/2}$. The solutions for E, P, B and D are smooth, sinusoidal-shape functions of ξ, and correspond to closed, periodic orbits in the (E, p)-phase plane.

5.3.2. Examples

The solution (5.45)–(5.49) yields smooth, periodic, traveling wave solutions, both for the case $0 < |s| < s_1$ and for the case $|s| > 1$. Fig. 7 shows the profiles of E, B, P and D as functions of ξ for $\alpha = 0.5$ and for two values of s. Fig. 7(a) gives an example of the traveling wave solution in the slow speed regime $0 < |s| < s_1$ for the case where $s = 0.5$. Fig. 7(b) gives an example of the wave in the fast speed regime $s > 1$ ($s = 1.01$ in the figure).

The solution for $s = 1.01$ in Fig. 7(b) has very large gradients E_ξ, every half period of the wave. It is straightforward to show that as $s \downarrow 1$, $|E_\xi| \to \infty$ at points on the profile where $E \approx 0$. This can be seen formally from the differential equation (5.40) for y. In the limit as $s \to 1$, $y_c \to 0$, and the ODE has a singularity at $y = 0$ ($\mathrm{d}y/\mathrm{d}\xi \propto y^{-1/2}$ as $y \to 0$). In the speed regime $s_2 < |s| < 1$, the traveling wave solution (5.45)–(5.49) develops an infinite gradient for E_ξ and the solution must involve shocks (i.e., either a finite jump in E, or $|E_\xi| \to \infty$ at $E = \pm E_c$ must occur on the solution profile). The profiles for E, B, and D in Fig. 7(b) are almost the same profile since $s \approx 1$, and exhibit steep gradients at points where $E \approx 0$. However the polarization P is smooth and has relatively small gradients.

5.3.3. Traveling waves for $s_2 < |s| < 1$

The solution (5.45) also applies in this case. In order to obtain a solution with $y_\xi^2 > 0$ requires that y be restricted to the range $0 < y < 3\alpha/2$. In this case it appears that one can obtain periodic travelling waves in which E is bounded, but with $|E_\xi| \to \infty$ as $y \to y_c$. Examples of solutions in which $|E_\xi| \to \infty$ as $E \to \pm E_c$ are described below.

Fig. 8(a) shows the traveling wave solution $E = E^{(+)} = E(\xi)$ obtained from (5.45)–(5.49) by varying ϕ from $\phi = -\pi/2$ to $\phi = \pi/2$ (the solid curve) for the case $s = 0.9$ and $\alpha = 0.5$. The dashed curve corresponds to the solution $E = E^{(-)} = -E(\xi)$. The solutions in Fig. 8(a) are clearly multi-valued. However, one can patch together pieces of the solutions $E = E^{(+)}$ and $E = E^{(-)}$ to produce the single valued wave profile in Fig. 8(b). This is achieved by noting that one can add a non-zero integration constant ξ_0, to the right hand side of (5.45), i.e.,

$$\xi = \xi^{(0)}(\phi) + \xi_0, \tag{5.50}$$

is also a solution of (5.40) where $\xi^{(0)}(\phi)$ is the solution (5.45). The solution in Fig. 8(b) has period

$$T_\xi = 2s\pi\left(3 - \frac{2}{\tau_0}\right) + 8|\xi_c|, \tag{5.51}$$

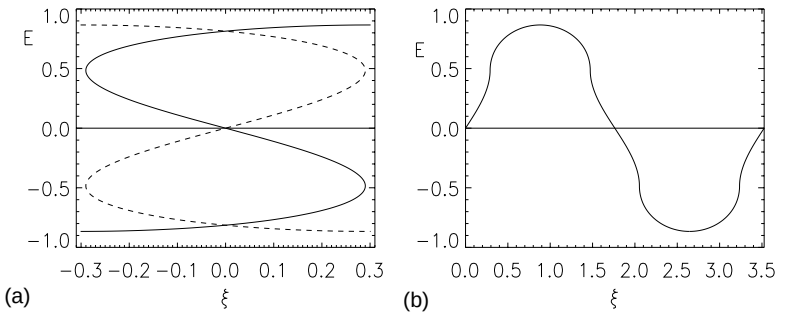

Fig. 8. (a) The solution for $E = E(\xi)$ obtained from the traveling wave solution (5.45)–(5.49) by varying the parameter ϕ from $\phi = -\pi/2$ to $\phi = \pi/2$, for the case $s = 0.9$ and $\alpha = 0.5$ (the solid curve). The dashed curve corresponds to the solution $E = -E(\xi)$. Panel (b) shows the solution for E obtained by patching together segments of the solutions in (a), with appropriate choices of the integration constant $\xi_0 = \xi_{0n}$ for the different solution segments. Note that $|E_\xi| \to \infty$ in both panels when $E = \pm E_c$.

where

$$\xi_c = s\left[3\phi_c - \frac{2}{\tau_0}\tan^{-1}\left(\frac{\tan\phi_c}{\tau_0}\right)\right], \tag{5.52}$$

is the point where $y = y_c$, $\tau = \tan\phi_c$, and $|E_\xi| \to \infty$. In the figure, $y_c = 0.23457$, $\phi_c = 34^\circ$ and $\xi_c = -0.29017$.

Fig. 9 shows the change in the waveform for E in Fig. 8(b) as the wave speed s increases. In Fig. 9(a), $s = 0.95$, whereas $s = 0.99$ in Fig. 9(b). The waveform in Fig. 9(b) is similar to the smooth, periodic waveform for E in Fig. 7(b) for $s = 1.01$, in which $|E_\xi|$ is bounded. Thus, the solutions in Figs. 8(b) and 9 can be regarded as the extension of the smooth traveling waves for $|s| > 1$ into the regime $s_2 < |s| < 1$, where the solutions exhibit gradient blowup at $E = \pm E_c$ (i.e., $|E_\xi| \to \infty$ at $E = \pm E_c$).

Clearly, other solutions with $|E_\xi| \to \infty$ as $E \to \pm E_c$ can be constructed. For example, the solutions in Figs. 8 and 9 only apply for $\tau_0 > 2/3$ (i.e. $|s| > s_4 = [5/(3\alpha + 5)]^{1/2}$). For $s = s_4$ the solution involves a cusp at the top of the profile for E. It also turns out that for $s = s_4$, the implicit solution (5.45) for $E(\xi)$ can be inverted, and an explicit solution for E as a function of ξ can be obtained. It is also worth noting that there exist classes of solutions of the form (5.41) with $s_1 < |s| < s_2$ with $y = E^2$ in the range $y_e < y < 3\alpha/2$ which exhibit gradient blowup (i.e., $|E_\xi| \to \infty$ as $E \to \pm E_c$).

The above solution examples, are representative of the type of traveling waves that are described in (5.30). However, the examples considered special cases where the function $\Phi(y)$ in the numerator had two equal, real roots. In these cases it is relatively easy to obtain analytical solutions of (5.30). More generally, the solution of (5.30)

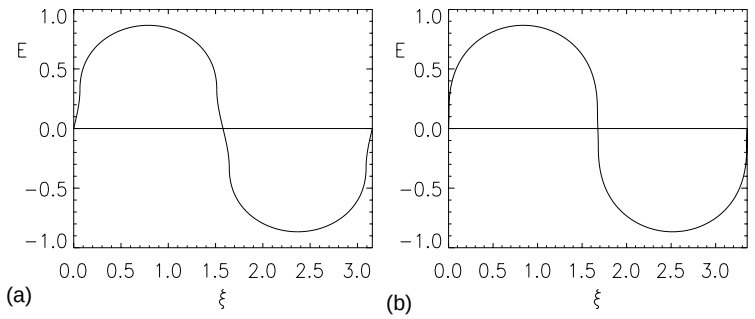

Fig. 9. The evolution of the waveform for E in Fig. 8(b) as s increases. In (a) $s = 0.95$ and in (b) $s = 0.99$. The parameter $\alpha = 0.5$.

depends on the character of the roots of the cubic $\Phi(y) = 0$. The discriminant of the cubic $\Phi(y) = 0$ [11, Formula 3.8.2, p. 17] can be written as:

$$D = \tfrac{1}{4}(\epsilon - \epsilon_{\rm cr})(\epsilon - \epsilon_{\rm h}), \tag{5.53}$$

where $\epsilon_{\rm cr}$ is the value (5.32) of ϵ for the critical solution, and $\epsilon_{\rm h}$ is the value (5.38) of ϵ for the heteroclinic solution. The roots of the cubic $\Phi(y) = 0$ are real and distinct if $D < 0$; there are three real roots, at least two of which are equal if $D = 0$ (i.e. if $\epsilon = \epsilon_{\rm cr}$ or $\epsilon = \epsilon_{\rm h}$); and there is one real root and two complex conjugate roots if $D > 0$. The main point we wish to emphasize here is that the type of solutions of (5.30) that can be obtained (i.e. smooth periodic solutions, or solutions with singularities at $E = \pm E_c$) depends on the discriminant D in (5.33). We note (without proof) that in the case of three real roots for $\Phi(y) = 0$, (5.30) can be integrated in terms of elliptic integrals.

6. Conclusions

The vector Maxwell equations coupled to a single Lorentz oscillator with instantaneous Kerr non-linearity were formulated in terms of Lagrangian and Hamiltonian variational principles. The canonical Hamiltonian description of the equations involves the solution of a polynomial equation for the electric field E, in terms of the canonical variables, with possible multiple real roots for E. In order to circumvent this problem, non-canonical Poisson bracket formulations of the equations are obtained in which the electric field is one of the non-canonical variables.

Using the Lie point symmetries admitted by the equations and Noether's theorem, we obtained four conservation laws for the equations. The symmetries were also used to obtain classical similarity solutions of the equations. The traveling wave similarity solutions were investigated using both Hamiltonian and non-Hamiltonian methods. In particular, the solutions in the case of a cubic Kerr non-linearity ($D = E + P + E^3/3$) were studied in detail. Two solutions of particular interest are: (i) the kink (or anti-kink) solution, which corresponds to a heteroclinic orbit connecting two saddle points in the (E, p)-phase plane, where E is the electric field, and p is the canonical momentum (the orbit can also be described in a similar way in the (q, p)-phase plane, where (q, p) are canonical coordinates) and (ii) the critical solution, which consists of a smooth, periodic traveling wave solution, which has the special property that the traveling wave ODE (5.30) has no singularities. For other solutions of (5.30), the ODE always has a singularity.

The traveling wave solutions were described using both canonical and non-canonical Poisson bracket descriptions. The canonical coordinates used to describe the traveling wave are $q = P$ and $p = P_\xi$, where P is the polarization electric field, and $\xi = z - st$ is the traveling wave variable. A non-canonical Poisson bracket description of the equations was also used, in which the non-canonical variables consisted of the electric field E and the canonical momentum p. This latter approach has the advantage that one does not need to solve a cubic for the electric field $E = E(q)$ in the analysis. For the case of a cubic, Kerr non-linearity, there are five critical points for the Hamiltonian in the (E, p)-phase plane. The solution trajectories in the (E, p) plane revealed four different possible solution topologies depending on the speed of the wave. Analysis of the critical, traveling wave solution, revealed that in the slowest speed regime, the solution has a very complicated trajectory in the (E, p)-phase plane. Numerical simulations revealed that this solution is unstable, in the sense that small perturbations of the critical solution lead to the formation of shocks. However, a more thorough stability analysis of this solution has not been carried out, and the stability of this solution is an open problem for further studies.

An investigation of the traveling wave solution (5.45) (which can be thought of as an extension of the heteroclinic solution), showed that smooth periodic solutions with speeds $|s| > 1$, develop very steep gradients E_ξ, as $|s| \downarrow 1$ (Fig. 7(b)). In fact the solution for $s = 1$ exhibits gradient blowup at points on the wave profile when $E = 0$ (in this case $E_c = 0$). It was demonstrated in Figs. 8 and 9, how the smooth solution with $|s| > 1$ could be extended into

the regime $(1+\alpha)^{-1/2} < |s| < 1$, where the solutions exhibit gradient blowup in E_ξ at points where $E = \pm E_c$. Other solutions which exhibit gradient blowup can also be constructed.

The travelling-wave kink and anti-kink solutions, which correspond to heteroclinic orbits in the (q, p) or (E, p)-phase planes, only exist for a restricted range of velocities s of the traveling wave. In this velocity range, the critical points in the (E, p)-phase plane consist of two saddles and three center critical points. The kink and anti-kink solutions correspond to the heteroclinic orbits connecting the two saddles. The numerical simulations indicated that the kinks are stable, but a more complete analytical proof of their stability has not been carried out.

Numerical simulations were also used to investigate the collision of kink anti-kink pairs. As a note on possible applications of the kink solutions we mention that kink anti-kink pairs form square like pulses, which in a communication system could represent the digit one. Absence of a square like pulse could represent the digit zero. However, the plateaus in the kinks have a finite value of the electric field and the polarization which means we need to store a rather substantial amount of energy in a fiber for utilizing kinks and anti-kinks in fiber communication systems. The advantages are extremely short and stable pulses.

Finally we mention that the kink solutions can switch the polarization from negative to positive or vice versa on an ultra fast time scale of the order few femto-seconds. This may be exploited in switching devices or in optical computing.

Acknowledgements

The work of GW was supported in part by NASA grant NAG5-10974. MPS wishes to thank the Arizona Center for Mathematical Sciences, where the bulk of this work was carried out. MPS acknowledges financial support from the Danish Technical Research Council through project number 56-00-0270. Part of this work has been supported by US Air Force Office of Scientific Research under contract nos. AFOSR-F49620-98-1-0227 and AFOSR-F49620-00-1-002.

Appendix A

In this appendix, we show that the non-canonical Poisson bracket (2.30) is skew-symmetric and satisfies the Jacobi identity. We use the notation:

$$P^\alpha = \frac{\delta \mathcal{P}}{\delta u^\alpha}, \qquad Q^\alpha = \frac{\delta \mathcal{Q}}{\delta u^\alpha}, \qquad R^\alpha = \frac{\delta \mathcal{R}}{\delta u^\alpha} \tag{A.1}$$

for the variational derivatives of the functionals $\mathcal{P}$, $\mathcal{Q}$ and $\mathcal{R}$. In the present analysis $u^\alpha \equiv \tilde{\eta}^\alpha$. The functional $\mathcal{P}[u]$ is of the form

$$\mathcal{P}[u] = \int_{-\infty}^{\infty} p[u]\,\mathrm{d}z, \tag{A.2}$$

and similarly for $\mathcal{Q}$ and $\mathcal{R}$. We require that the Poisson bracket (2.30) satisfy the conditions of skew-symmetry ($\{\mathcal{P}, \mathcal{Q}\} = -\{\mathcal{Q}, \mathcal{P}\}$) and the Jacobi identity:

$$\mathcal{I}(\mathcal{P}, \mathcal{Q}, \mathcal{R}) \equiv \{\{\mathcal{P}, \mathcal{Q}\}, \mathcal{R}\} + \{\{\mathcal{Q}, \mathcal{R}\}, \mathcal{P}\} + \{\{\mathcal{R}, \mathcal{P}\}, \mathcal{Q}\} = 0. \tag{A.3}$$

To prove skew-symmetry of the bracket, we note from (2.30) that:

$$\begin{aligned}\{\mathcal{P},\mathcal{Q}\} &= \int_{-\infty}^{\infty} \mathrm{d}z (P^1, P^2, P^3, P^4)\cdot(-\zeta D_z Q^2 - \zeta Q^4, -D_z(\zeta Q^1), Q^4, \zeta Q^1 - Q^3)^{\mathrm{T}} \\ &\equiv -\int_{-\infty}^{\infty} \mathrm{d}z \{D_z[\zeta(P^1 Q^2 + P^2 Q^1)] \\ &\quad + (Q^1, Q^2, Q^3, Q^4)\cdot(-\zeta D_z P^2 - \zeta P^4, -D_z(\zeta P^1), P^4, \zeta P^1 - P^3)^{\mathrm{T}}\}. \end{aligned} \tag{A.4}$$

Assuming $|\zeta(P^1 Q^2 + P^2 Q^1)| \to 0$ as $|z| \to \infty$, (A.4) reduces to the equation $\{\mathcal{P},\mathcal{Q}\} = -\{\mathcal{Q},\mathcal{P}\}$, which proves the skew-symmetry of the bracket.

To prove that the Jacobi identity is satisfied, we note from [8, Eq. (7.11)], that the Jacobi identity (A.3) is equivalent to:

$$\mathcal{I}(\mathcal{P},\mathcal{Q},\mathcal{R}) = \int_{-\infty}^{\infty} \mathrm{d}z [\mathbf{P}\cdot\hat{X}[\tilde{\mathbf{J}}\mathbf{R}](\tilde{\mathbf{J}})\cdot\mathbf{Q} + \mathbf{R}\cdot\hat{X}[\tilde{\mathbf{J}}\mathbf{Q}](\tilde{\mathbf{J}})\cdot\mathbf{P} + \mathbf{Q}\cdot\hat{X}[\tilde{\mathbf{J}}\mathbf{P}](\tilde{\mathbf{J}})\cdot\mathbf{R}] = 0, \tag{A.5}$$

where $\hat{X}[\hat{\phi}]$ is the prolonged, canonical symmetry operator (3.10) (note that $\hat{X}[\hat{\phi}]$ would be written as $\mathrm{pr}\,\hat{V}_{\hat{\phi}}$ in Olver's notation). The first term in (A.5) can be expanded as:

$$\begin{aligned}\int_{-\infty}^{\infty} \mathbf{P}\cdot\hat{X}[\tilde{\mathbf{J}}\mathbf{R}](\tilde{\mathbf{J}})\cdot\mathbf{Q}\,\mathrm{d}z &= \int_{-\infty}^{\infty} \mathrm{d}z [P^1[\zeta\zeta'(D_z R^2 + R^4)(D_z Q^2 + Q^4)] + P^2 D_z[(D_z R^2 + R^4)\zeta\zeta' Q^1] \\ &\quad - P^4(D_z R^2 + R^4)\zeta\zeta' Q^1], \end{aligned} \tag{A.6}$$

where $\zeta' = \mathrm{d}\zeta/\mathrm{d}E$ and ζ is given in (2.32). Similar expressions for the other two terms in (A.5) can be obtained by cyclically permuting P, Q and R in (A.6). Adding the three resultant expressions analogous to (A.6) and (A.5) reduces to:

$$\mathcal{I}(\mathcal{P},\mathcal{Q},\mathcal{R}) = \int_{-\infty}^{\infty} D_z(\Lambda)\,\mathrm{d}z, \tag{A.7}$$

where

$$\Lambda = \zeta\zeta'[Q^1 P^2(D_z R^2 + R^4) + R^1 Q^2(D_z P^2 + P^4) + P^1 R^2(D_z Q^2 + Q^4)]. \tag{A.8}$$

Thus, assuming $\Lambda \to 0$ as $|z| \to \infty$ we find $\mathcal{I}(\mathcal{P},\mathcal{Q},\mathcal{R}) = 0$, which proves the Jacobi identity (A.3). In the above analysis, the integrals involved are assumed to converge, and are well defined. It should be noted that certain surface terms analogous to Λ are assumed to vanish in the derivation of the condition (A.5) from the Jacobi identity (A.3).

References

[1] C.V. Hile, Comparisons between Maxwell's equations and an extended nonlinear Schrödinger equation, Wave Motion 24 (1996) 1–12.
[2] M.P. Sørenson, M. Brio, G.M. Webb, J.V. Moloney, Solitary waves, steepening and initial collapse in the Maxwell–Lorentz system, Physica D 170 (2002) 287–303.
[3] L. Gilles, J.V. Moloney, L. Vázquez, Electromagnetic shocks on the optical cycle of ultrashort pulses in triple-resonance Lorentz dielectric media with subfemtosecond nonlinear electronic Debye relaxation, Phys. Rev. E 60 (1) (1999) 1051–1059.
[4] L. Gilles, S.C. Hagness, L. Vázquez, Comparison between staggered and unstaggered finite-difference time-domain grids for few-cycle temporal optical soliton propagation, J. Comput. Phys. 161 (2000) 379–400.
[5] I.N. Bronstein, K.A. Semendjajew, Taschenbuch der Mathematik, Verlag Harri Deutsch, Thun, 1989.
[6] K.R. Jackson, Runge–Kutta solver DVERK. http://www.netlib.org.
[7] G.W. Bluman, S. Kumei, Symmetries and Differential Equations, Springer Verlag, New York, 1989.
[8] P.J. Olver, Applications of Lie Groups to Differential Equations, 2nd ed., Springer Verlag, New York, 1993.
[9] L.V. Ovsjannikov, Group Analysis of Differential Equations, Academic Press, New York, 1982.

[10] N.H. Ibragimov, Transformation Groups Applied to Mathematical Physics, Reidel, Dordrecht, 1985.
[11] M. Abramowitz, I.A. Stegun, Handbook of Mathematical Functions, Dover, New York, 1965.
[12] P.E. Hydon, Symmetry Methods for Differential Equations, Cambridge University Press, Cambridge, UK, 2000.
[13] H. Goldstein, Classical Mechanics, 2nd ed., Addison-Wesley, Reading, MA, 1980.
[14] R.L. Dewar, Energy–momentum tensors for dispersive electromagnetic waves, Aust. J. Phys. 30 (1977) 533–575.
[15] G.W. Bluman, J.D. Cole, The general similarity solution of the heat equation, J. Math. Mech. 18 (1969) 1025–1042.
[16] G. Birkhoff, S. MacLane, A Survey of Modern Algebra, 3rd ed., MacMillan, New York, 1965.
[17] F. Magri, An operator approach to Poisson brackets, Ann. Phys. 99 (1976) 196–228.
[18] F. Magri, A simple model of the integrable Hamiltonian equation, J. Math. Phys. 19 (1978) 1156–1162.
[19] J.E. Marsden, T.S. Ratiu, Introduction to Mechanics and Symmetry, Springer, New York, 1994.
[20] V.E. Zakharov, E.A. Kuznetsov, A Hamiltonian formalism for systems of hydrodynamic type, Sov. Sci. Rev. C: Math. Phys. Rev. 4 (1984) 167–219.
[21] J.E. Marsden, A. Weinstein, Coadjoint orbits, vortices and Clebsch variables for incompressible fluids, Physica D 7 (1983) 305–323.
[22] P.J. Morrison, Poisson brackets for fluids and plasmas, in: M. Tabor, Y. Treve (Eds.), Mathematical Methods in Hydrodynamics and Integrability in Related Dynamical Systems, Proceedings of the Conference on AIP, vol. 88, 1982, pp. 13–26.
[23] P.J. Morrison, Hamiltonian description of the ideal fluid, Rev. Mod. Phys. 70 (1998) 467–521.
[24] B.K. Harrison, F.B. Estabrook, Geometric approach to invariance groups and solution of partial differential systems, J. Math. Phys. 12 (1971) 653–666.
[25] H.D. Wahlquist, F.B. Estabrook, Prolongation structure of nonlinear evolution equations, J. Math. Phys. 16 (1975) 1–7.
[26] T.E. Holzer, W.I. Axford, The theory of stellar winds and related flows, Ann. Rev. Astron. Astrophys. 8 (1970) 31.